Solar Physics
DOI: 10.1007/•••••-•••-•••-••••-•

Relationships between the Spectra of near-Earth Proton Enhancements, Hard X-Ray Bursts, and CME Speeds

V.I. Kiselev · N.S. Meshalkina · V.V. Grechnev

Received ; accepted

Abstract Some studies propose the transfer of flare-accelerated protons in an erupting flux rope until its reconnection with an open structure releases the trapped protons. Coulomb collisions in the dense flux-rope body deplete the low-energy part of the proton spectrum. On the other hand, shock-acceleration progressively replenishes this spectral part. These processes form a double power-law proton spectrum that is usually observed in the Earth orbit. We analyze the correlations between the slopes of near-Earth proton spectra below and above the break energy, on the one hand, and photon indices of the corresponding hard X-ray (HXR) bursts and speeds of associated coronal mass ejections (CMEs), on the other hand. We use catalogs of proton events in 1991–2006, HXR spectra obtained by Yohkoh and the Reuven Ramaty High-Energy Solar Spectroscopic Imager (RHESSI), and CME catalogs. Significant correlations have been found between the proton spectral slopes i) above the break energy and HXR spectral indices (0.86), and ii) below the break energy and CME speeds (−0.75). The results indicate a statistical predominance of flare-acceleration at higher proton energies and shock-acceleration at their lower energies. The highest-energy proton spectra reconstructed in ground-level events exhibit the second break with a steepest slope above it. Neither this slope nor the second-break energy correlates with any other parameter. This particularity needs understanding.

Keywords: Coronal Mass Ejections; Energetic Particles, Protons; X-Ray Bursts, Hard

✉ V.I. Kiselev
valentin_kiselev@iszf.irk.ru

N.S. Meshalkina
nata@iszf.irk.ru

V.V. Grechnev
grechnev@iszf.irk.ru

Institute of Solar-Terrestrial Physics SB RAS, Lermontov St. 126A, Irkutsk 664033, Russia

1. Introduction

Solar energetic particles (SEPs) pose a threat to the equipment of spaceships, astronauts, and even crew members and passengers of transcontinental flights. The acceleration mechanisms of SEPs offer a long-standing challenge for basic physics. Two main categories of SEP events have been identified several decades ago (e.g. Croom, 1971; Cliver et al., 1989), i.e. electron-rich impulsive events accompanied by Type III radio bursts and proton-rich gradual events accompanied by coronal mass ejections (CMEs) and Type II bursts. Over the next decades, several other differences have been found between impulsive and gradual events (e.g. Reames, 2013).

The acceleration of electrons in flares has undoubtedly been revealed long ago (e.g. Kane, 1974), although it is still difficult to consider specific acceleration mechanisms established. The origin of accelerated protons and heavier ions is even more obscure. One of their possible sources is related to flare processes in an active region (e.g. Klein and Trottet, 2001; Kallenrode, 2003; Grechnev et al., 2008, 2015; Aschwanden, 2012). Another probable accelerator of protons is a CME-associated shock wave that is traditionally presumed to be a bow shock driven by a super-Alfvénic CME (e.g. Kahler, 1982; Reames, 2009; Gopalswamy et al., 2012; Cliver, 2016; Kahler et al., 2017; Cliver et al., 2019). Unlike accelerated electrons that are directly manifested in a wide range of electromagnetic emission, accelerated protons can be detected only in situ or from remote observations by addressing indirect manifestations. Considerations often involve unverified assumptions such as the shock formation when a CME becomes super-Alfvénic and the onset of a Type II burst at that time; both are invoked in the interpretation of the proton release time (e.g. Reames, 2009; Gopalswamy et al., 2013). Difficulties in identifying the sources of accelerated protons are aggravated by the fact that considerable proton fluxes are usually observed after major solar eruptive events associated with both strong flares and fast CMEs, which complicates untangling their contributions.

Much effort has been made to identify the elusive source of accelerated solar protons from various statistical indications, analyzing the correlations between the fluxes of flare emissions and CME, on the one hand, and proton fluxes observed near Earth, on the other hand. In particular, the association of proton events with strong high-frequency radio bursts has been known for several decades (e.g. Croom, 1971; Castelli and Barron, 1977; Akinian et al., 1978; Melnikov et al., 1991). Alternatively, Kahler (1982) argued that a general correspondence between the energy release in a big eruptive flare and its various manifestations should lead to a correlation between different parameters, regardless of any physical connection between them. He also emphasized the importance of matching the spectral characteristics of near-Earth protons and in their source, but found a poor correlation between the microwave peak frequency and peak proton flux. Note that the relationship between the parameters of accelerated electrons and the gyrosynchrotron emission that they produce is not straightforward even for a simplest source (Dulk and Marsh, 1982), having additionally a strong dependence on magnetic field. It is still more complicated for a real flare arcade, depending on the symmetry of the magnetic configuration (Grechnev

et al., 2017b). Indications have been reported of a trend linking the spectral parameters of microwave bursts and proton events (Chertok, 1990; Chertok, Grechnev, and Meshalkina, 2009; Grechnev et al., 2013b), but they do not appear to be decisive. For example, the trend between the ratio of flux densities at the frequencies of 9 and 15 GHz and the proton spectral hardness is too loose to be used alone in forecasting procedures (Chertok, Grechnev, and Meshalkina, 2009; Núñez et al., 2018).

The results of different case studies and statistical analysis are ambiguous; some of them favor one option, while others another. For example, γ-ray bursts observed in the flare impulsive phase and high-energy neutrons, which are detected starting at this time in rare events, indicate flare-acceleration of protons (Kuznetsov et al., 2006, 2011, 2014; Chupp and Ryan, 2009; Vilmer, MacKinnon, and Hurford, 2011; Yu et al., 2015). On the other hand, in situ measurements of the SEP composition, such as the iron charge state, the ^{3}He/^{4}He, H/He, and Fe/O ratios, and some other properties of ions produced in gradual events, indicate their shock-acceleration (e.g. Tylka et al., 2005; Reames, 2013). Overall, these circumstances leave the impression that both flares and shock waves are involved in the acceleration of heavy particles, while different observables and energy ranges indicate their different origins. The statistical studies by Dierckxsens et al. (2015), Trottet et al. (2015), and Papaioannou et al. (2016) do indeed support the conclusion by Klein and Trottet (2001) that shock-acceleration dominates at the lower proton energies, while flare-related acceleration dominates at high energies.

To find a possible key to the problem, consider the scenario proposed by Masson, Antiochos, and DeVore (2013). In this scenario, flare-accelerated electrons and protons are injected from the acceleration region both down, into the flare loops, and up, into the forming flux rope. There they get trapped until the expanding flux rope reconnects with an open coronal structure, releasing the trapped particles into the interplanetary space. This scenario was supported by Kocharov et al. (2017) and elaborated by Grechnev et al. (2017a). Coulomb collisions in the dense flux-rope body deplete the low-energy part of the proton spectrum. On the other hand, the CME-associated shock independently accelerates a seed population of suprathermals existing in the corona and interplanetary space, progressively elevating their spectrum to higher energies and replenishing the low-energy spectral part. As a result of the two processes, one might expect a double power-law proton spectrum with a flatter slope below the break energy and a steeper slope above it. Such spectra are indeed commonly observed in the range from the lowest proton energies to several hundred MeV (e.g. Mewaldt et al., 2012 and other studies referenced therein). The following forms are involved in the analysis of the spectra.

Ellison and Ramaty (1985) deduced for shock-accelerated SEPs the differential spectrum in the form of a power-law with an exponential rollover (we consider all spectral indices to be positive):

$$\mathrm{d}J/\mathrm{d}E = K(E/E_\mathrm{r})^{-\gamma}\exp(-E/E_0) \tag{1}$$

with $[J]$ being intensity or fluence, $[E]$ kinetic energy, $K = A_\mathrm{r}\exp(E_\mathrm{r}/E_0)$, $[A_\mathrm{r}]$ normalization constant at a reference energy $[E_\mathrm{r}]$, $[\gamma]$ the power-law index, and

[E_0] the rollover energy. Tylka et al. (2005), Mewaldt et al. (2012), and other studies they mentioned concluded that event-integrated fluence spectra in this energy range fit best with a double power-law function that was initially proposed by Band et al. (1993) for fitting γ-ray burst spectra. This function combines the Ellison–Ramaty pattern at lower energies with the second, steeper power-law at higher energies:

$$\begin{aligned} \mathrm{d}J/\mathrm{d}E &= K(E/E_\mathrm{r})^{-\gamma_1} \exp(-E/E_0) \text{ for } E \le (\gamma_2 - \gamma_1)E_0; \\ \mathrm{d}J/\mathrm{d}E &= K(E/E_\mathrm{r})^{-\gamma_2}[(\gamma_2 - \gamma_1)E_0/E_\mathrm{r}]^{(\gamma_2-\gamma_1)} \exp(\gamma_1 - \gamma_2) \text{ for } E > (\gamma_2 - \gamma_1)E_0, \end{aligned} \quad (2)$$

where [γ_1] is the low-energy power-law slope and [γ_2] is the high-energy power-law slope. Mewaldt et al. (2012) found that the break energies range from units to tens of MeV in large SEP events they considered.

There is a possibility to reveal correlations between the slopes of the spectra of near-Earth proton enhancements above the break energy and below it, on the one hand, and parameters of their solar sources, on the other hand. At present, this is possible due to many years of observations of both CMEs by the Large Angle Spectroscopic Coronagraph (LASCO: Brueckner et al., 1995) on board the Solar and Heliospheric Observatory (SOHO: Domingo, Fleck, and Poland, 1995) since 1996, and hard X-ray (HXR) flare emission. The latter was observed particularly by the Hard X-ray Spectrometer (HXS: Yoshimori et al., 1991) of the Yohkoh mission (Ogawara et al., 1991) in 1991–2001 and by the Reuven Ramaty High-Energy Solar Spectroscopic Imager (RHESSI: Lin et al., 2002) in 2002–2018. The advantage of this approach over the previous analysis of microwave bursts lies in the direct relation of thick-target bremsstrahlung to the parameters of accelerated electrons, although Hannah and Kontar (2011) warn that sometimes the thick-target model does not match observations perfectly.

We are aware of two similar statistical studies by Tripathi et al. (2013) and by Bhatt, Jain, and Awasthi (2013). Both studies used seven-channel data (from 0.8–4 MeV to 165–500 MeV) produced by the proton detectors on board the Geostationary Operation Environmental Satellites (GOES) that were fitted with a single power-law. By combining input data into bins (binning) to reduce the scatter, Tripathi et al. (2013) found a correlation coefficient [ρ] of -0.71 between the proton index and the CME speed, and $\rho \approx 0.8$ between the proton index and the HXR index, while without the binning the correlations were weak, with $|\rho| \approx 0.5$. Instead the binning of data, Bhatt, Jain, and Awasthi (2013) considered the hardest spectral indices over each flare and over an SEP event. For 12 events, which produced sufficient responses in the seven GOES channels to yield satisfactory spectra, they found the correlation coefficients between the HXR and proton spectral indices of $\rho \approx 0.9$ (in our impression, it is closer to 0.69 that is also significant) and between the CME speed and the proton index $\rho \approx 0.96$. However, the impressive results of the two studies are unlikely to help in separating the flare-related and shock-related contributions, which is expected when using the double power-law fit of the proton spectra.

Our initial intention was to analyze SEP events, whose spectra are available in the catalog of solar proton events in Solar Cycle 23 (1996–2006) composed by Logachev et al. (2016), and whose associated flares were observed by RHESSI.

These events fall into the interval from 2002 through 2006. Then we found that RHESSI missed a number of events, some flares were occulted, or other reasons prevented their analysis. This circumstance considerably reduced the number of analyzed events and prompted us to expand the analysis to the earlier events observed by Yohkoh in 1991–2001. The spectra of proton events that occurred in 1991–1995 are contained in the catalog composed by Sladkova et al. (1998), where the data are less detailed than in the catalog by Logachev et al. (2016).

Our analysis is aimed at the following goals: i) to estimate the slopes of the near-Earth proton spectra below the break energy [$\gamma_{\rm p1}$] and above it [$\gamma_{\rm p2}$], ii) to evaluate the correlations between the slopes of the spectra of protons, the HXR index [$\gamma_{\rm HXR}$] in associated flares, and CME speeds [$V_{\rm CME}$], iii) to identify the components of the proton spectra caused by the flare-acceleration and shock-acceleration, and iv) to verify the scenario of the flux-rope-mediated transfer of flare-accelerated protons. Ultimately, we endeavor to take a step towards clarifying the origin of SEPs and to show the possibility of reconciling the conclusions of different studies when they seem to contradict each other.

Section 2 describes input data, their selection, preparation and processing, and presents the results. Section 3 addresses the statistical relationships between the spectral parameters of near-Earth proton enhancements, HXR emission, and CME speeds. Section 4 discusses the results and their implications. Section 5 summarizes the main outcome of the study. Section A in Appendix lists the events excluded from the analysis.

2. Preparation of Input Data for Statistical Analysis

2.1. Proton Events and Spectra

For the analysis we selected 15 events observed by RHESSI that are listed in Table 1 and 15 events observed by Yohkoh that are listed in Table 2. The events were selected from the catalogs of proton events by Logachev et al. (2016) and by Sladkova et al. (1998) that are accessible at www.wdcb.ru/stp/solar/solar_proton_events.html. The catalogs present the time-of-maximum integral spectra of solar proton events compiled from data of detectors on board several missions and characterize their probable solar sources. At the first step, we tentatively selected from these catalogs 94 candidate proton events, whose solar sources were reliably identified.

A number of reasons forced us to exclude a considerable number of events from the analysis. These were, for example, the night of spacecraft or its location in the South-Atlantic Anomaly (SAA), where observations were interrupted because of high background radiation; the flare position behind the limb or nearby, so that it may be partly occulted; data issues, etc. Excluded events and reasons for their exclusion are listed in Tables 3 and 4 in Appendix. The final selection reduced the number of events by more than three times.

We adopt the conclusion of Mewaldt et al. (2012) and other studies that the observed proton spectra fit best with a double power-law shape. This spectral

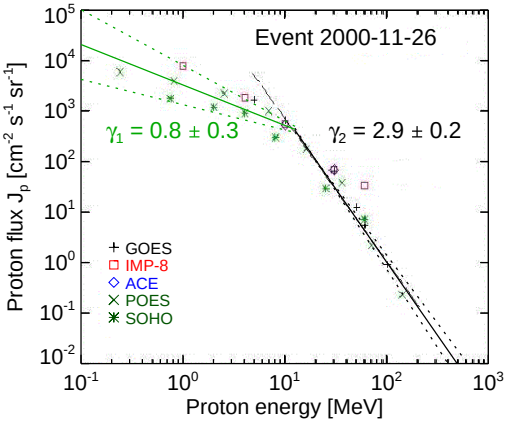

Figure 1. The time-of-maximum integral spectrum of the near-Earth proton enhancement on 26 November 2000 (symbols) presented in the catalog by Logachev et al. (2016) along with fitting of its low-energy and high-energy branches (solid lines). The dotted lines represent the uncertainties in the spectral slopes.

shape meets our expectations of two different spectral slopes to the left of the break energy [γ_{p1}] and to the right of it [γ_{p2}] that are independent of each other.

The slopes of a spectrum taken from a catalog of solar proton events were estimated by manual linear fitting of each of its corresponding branch. An example of a time-of-maximum integral spectrum of the near-Earth proton enhancement on 26 November 2000 with a single break-energy point (Logachev et al., 2016) is shown in Figure 1. Uncertainties of the proton power-law indices were estimated visually by varying the fit. In case of discrepancies between the data, for example, the IMP-8 points in the range of 30–60 MeV in Figure 1, preference was given to other detectors with a larger number of points that were consistent with each other (here GOES, POES, and SOHO points in the same range). The energy breakpoints (determined by the intersection of the two power laws) in all thirty analyzed spectra are in the range from about 3 MeV to 63 MeV. The break energies do not correlate with either [γ_{p1}] or [γ_{p2}].

2.2. Hard X-ray Spectra

The RHESSI browser at sprg.ssl.berkeley.edu/~tohban/browser/?show=qli was used to preview RHESSI data and to check if the observation was acceptable. RHESSI data were retrieved and processed using standard software. The measurements of the HXR spectral index with uncertainties from RHESSI data (and Konus-WIND data as well) were performed by means of the Object Spectral Executive software (OSPEX: Tolbert and Schwartz, 2020; hesperia.gsfc.nasa.gov/ssw/packages/spex/doc/ospex_explanation.htm) that is an object-oriented interface for X-ray spectral analysis of solar data commonly used in recent studies (e.g. Bhatt, Jain, and Awasthi, 2013; Share et al., 2018). In our measurements, the timing of an HXR peak is critical. We selected the strongest and hardest peak (detectable at the highest energies) and estimated its occurrence time by referring to the 50–100 keV and the higher-energy RHESSI channels.

We are interested in particles of sufficiently high energies, whose presumable injection into the forming flux rope should be accompanied by the precipitation of electrons down, into dense layers of the solar atmosphere, producing bremsstrahlung pulses of a relatively short duration. We computed the HXR spectra from RHESSI data with an integration time of 30 seconds centered on an HXR peak. This time is usually too short to accumulate a sufficient number of counts to obtain satisfactory spectra at several hundred keV. Also, nuclear emissions begin to appear at higher energies, flattening the total spectrum. We assume that the electron bremsstrahlung spectral component has a single power-law shape in the entire range from the low-energy cutoff up to the high-energy rollover (same as Equation 1) that is widely used (e.g. Miller and Ramaty, 1989; Ackermann et al., 2014; Ajello et al., 2021). In order to maintain uniformity in the spectral analysis of all flares from our list of candidate events and to avoid the issues of detector cross-calibration, we used data from detector 4, following recommendations by Smith et al. (2002).

Before fitting the spectra, the observed counts were corrected for pulse pileup and decimation. We estimated the photon index [$\gamma_{\rm HXR}$] and its errors, employing the standard spectral analysis techniques for RHESSI data. The spatially-integrated count flux spectra were fitted between 3 and 250 keV using a combination of variable thermal (vth) and triple power-law (3pow) models for all events. The initial spectral fit yielded a number of free parameters of the vth + 3pow model that were varied until a reasonably good fit was achieved. The systematic uncertainty was set between 0 and 0.1 so that the model fitted the observed spectra with $\chi^2 < 3$. We required that [$\gamma_{\rm HXR}$] obtained by forward fitting of an HXR spectrum in the energy range between 50 and 200 keV fall in the range from 2.5 to 4.5. If the result did not meet this condition, then the situation was investigated; the comparison with quick-look spectra available at the RHESSI browser was also used herewith. The reason for the questionable value of [$\gamma_{\rm HXR}$] was identified and either the HXR peak time was refined, or significant reasons were found to exclude the event from the analysis.

The HXR spectral indices estimated in this way from RHESSI data are listed in Table 1. The only exception is event 2 (SOL2003-06-17), where a few HXR peaks occurred; here we averaged the results of a detailed study of this event by Kundu et al. (2009). Excluded events are listed in Table 3 in Appendix.

For the events that occurred in 1991–2001, we used the Yohkoh/HXS spectra from the catalog by Sato et al. (2006). The accumulation intervals chosen by the authors in most cases cover the strongest and hardest HXR peak. We fitted the spectra with a single power law in the energy range of about 100–300 keV manually and estimated the uncertainties visually. An example of a photon spectrum recorded by Yohkoh/HXS on 25 November 2000 along with its fit is shown in Figure 2. The HXR spectral indices estimated from Yohkoh data are listed in Table 2 and excluded events are listed in Table 4 in Appendix.

The search for data of the Konus Gamma-Ray Burst Experiment (Konus-Wind: Aptekar et al., 1995) on board the Wind mission did not reveal any additional events other than those observed by RHESSI or Yohkoh. The estimates of the HXR photon index from the Konus-Wind data are generally consistent with RHESSI data, although with larger uncertainties. After previewing the Konus-Wind data, we did not use them in the study.

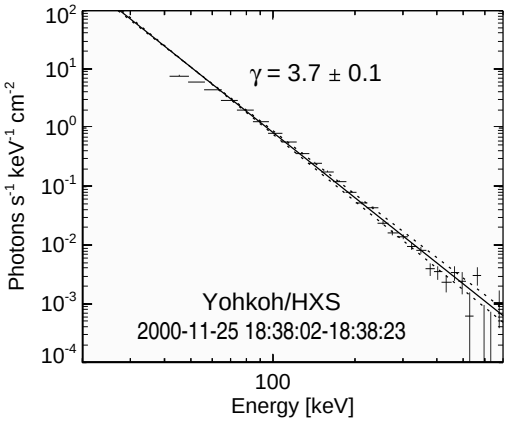

Figure 2. The photon spectrum recorded by Yohkoh/HXS on 25 November 2000 (Sato et al., 2006) along with its fit (solid line). The dotted lines represent the uncertainties in the spectral slope.

2.3. Data for Statistical Analysis

We mostly used the average (linear-fit) CME speeds from the online CME catalog (Yashiro et al., 2004: cdaw.gsfc.nasa.gov/CME_list/) that is based on the measurements from SOHO/LASCO observations. This catalog was also used to check the association of a CME with an event in question. In addition, we considered deprojected CME speeds (radial or "space speeds") evaluated in the online halo CME catalog cdaw.gsfc.nasa.gov/CME_list/HALO/. These catalogs contain CMEs observed from January 1996 up to the present, with a break from July to mid-October 1998. We have no data on CMEs before 1996 and during the interruption of SOHO observations in 1998.

Tables 1 and 2 present the parameters of the proton events, associated flares, and CME speeds that we use in our statistical analysis. The left part of Table 1 lists the number of event, the flare date in the format of the Solar Object Locator (yyyy-mm-dd), the GOES peak time and class, the estimated HXR spectral index [$\gamma_{\rm HXR}$], and the flare position. The middle column lists the average plane-of-the-sky (POS) and radial (rad) CME speed. The right part of Table 1 lists the peak time of a near-Earth proton enhancement, the break energy E_0, and the proton spectral indices below it [$\gamma_{\rm p1}$] and above it [$\gamma_{\rm p2}$]. The structure of Table 2 is mainly identical to that of Table 1, but the fifth column presents the temporal intervals of the measured Yohkoh spectra instead of the times of HXR peaks. Unknown or uncertain parameters are denoted "ND" in all tables.

Table 1. Events analyzed using RHESSI data.

No.	Solar flare						$V_{\rm CME}$	Near-Earth protons			
	Date	GOES peak	GOES class	RHESSI peak	$\gamma_{\rm HXR}$	Position	POS/rad [km s^{-1}]	Peak time	E_0 [MeV]	$\gamma_{\rm p1}$	$\gamma_{\rm p2}$
1	2002-11-09	13:23	M4.6	13:16:32	3.77 ± 0.21	S04 W29	1757/2159	10/02:00	9 ± 2	0.6 ± 0.2	2.7 ± 0.2
2	2003-06-17	22:55	M6.8	22:46:20	3.31 ± 0.25[a]	S12 E60	1779/1918	19/06:00	5 ± 1	0.7 ± 0.2	2.7 ± 0.4
3	2003-10-29[b]	20:49	X10	20:46:00	3.26 ± 0.01	S15 W02	1948/2628	29/23:00	33 ± 6	0.7 ± 0.2	2.2 ± 0.2
4	2003-11-02[b]	17:25	X8.3	17:16:53	2.83 ± 0.02	S14 W56	1826/2733	02/23:00	16 ± 4	0.5 ± 0.3	1.7 ± 0.4
5	2003-11-20	23:53	M5.8	23:49:09	3.70 ± 0.20	N02 W17	547/1173	22/02:00	3 ± 1	0.7 ± 0.1	2.5 ± 0.3
6	2004-04-11	04:19	C9.6	04:15:36	3.54 ± 0.01	S14 W47	1645/1645	11/12:00	6 ± 2	0.6 ± 0.2	3.0 ± 0.3
7	2004-09-12	00:56	M4.8	00:33:51	3.73 ± 0.20	N04 E42	1150/1436	13/23:00	5 ± 1	0.6 ± 0.2	3.4 ± 0.3
8	2004-09-19	17:12	M1.9	16:57:04	3.89 ± 0.10	N03 W60	ND[c]	20/01:00	20 ± 5	0.5 ± 0.3	2.9 ± 0.4
9	2004-11-10	02:13	X2.5	02:09:49	3.32 ± 0.01	N07 W51	1975/3656	10/16:00	9 ± 2	0.5 ± 0.2	2.5 ± 0.2
10	2005-01-15	23:02	X2.6	22:48:12	3.52 ± 0.32	N14 W08	2861/3682	16/18:00	9 ± 1	0.5 ± 0.3	2.1 ± 0.3
11	2005-01-17[b]	09:52	X3.8	09:43:29	3.74 ± 0.14	N14 W24	2547/3029	17/17:00	28 ± 7	0.6 ± 0.2	2.8 ± 0.4
12	2005-01-20[b]	07:01	X7.1	06:46:07	3.05 ± 0.24	N12 W58	2800/2900	20/10:00	46 ± 5	0.5 ± 0.3	1.6 ± 0.3
13	2005-05-13	16:57	M8.0	16:42:03	3.59 ± 0.20	N12 E12	1689/2171	14/14:00	8 ± 2	0.7 ± 0.4	3.2 ± 0.3
14	2005-07-30	06:35	X1.3	06:32:29	3.69 ± 0.01	N12 E61	1968/2043	01/05:00	4 ± 1	0.8 ± 0.3	3.3 ± 0.4
15	2006-12-06	18:47	X6.5	18:43:40	3.23 ± 0.01	S06 E63	ND	07/22:00	12 ± 1	0.5 ± 0.2	2.3 ± 0.2

[a] Multiple peaks; the results of Kundu et al. (2009) are used
[b] Event associated with a ground-level enhancement (GLE)
[c] No data

Table 2. Events analyzed using Yohkoh data.

No.	Solar flare						V_{CME}	Near-Earth protons			
	Date	GOES peak	GOES class	Yohkoh measured interval	γ_{HXR}	Position	POS/rad [km s^{-1}]	Peak time	E_0 [MeV]	γ_{p1}	γ_{p2}
1	1991-11-15	22:40	X1.5	22:37:06–22:37:34	3.4 ± 0.2	S13 W19	ND[c]	16/03:00	40 ± 10	1.2 ± 0.3	2.2 ± 0.3
2	1992-11-23	20:32	M4.4	20:24:12–20:25:57	3.5 ± 0.2	S08 W89	ND	23/23:00	30 ± 5	2.2 ± 0.2	2.9 ± 0.1
3	1993-06-07	14:25	M5.4	14:21:02–14:22:12	3.9 ± 0.2	S10 W30	ND	07/16:00	30 ± 7	1.8 ± 0.2	3.5 ± 0.1
4	1997-11-06[b]	11:56	X9.4	11:55:20–11:55:48	3.2 ± 0.1	S18 W63	1556/1604	07/02:00	31 ± 4	0.7 ± 0.2	1.7 ± 0.1
5	1998-05-02[b]	13:42	X1.1	13:37:18–13:37:38	3.2 ± 0.2	S15 W15	938/1168	02/16:00	63 ± 10	0.8 ± 0.3	2.3 ± 0.2
6	1998-05-06[b]	08:09	X2.7	08:03:29–08:03:44	3.3 ± 0.1	S15 W64	1099/1099	06/09:00	21 ± 6	0.7 ± 0.2	2.1 ± 0.2
7	1998-05-09	03:40	M7.7	03:22:55–03:24:05	3.5 ± 0.1	S15 W90	2331/2331	09/13:00	22 ± 5	0.6 ± 0.2	2.3 ± 0.1
8	1998-11-05	19:55	M8.4	19:43:35–19:43:53	3.5 ± 0.1	N22 W18	1118/1335	06/12:00	3 ± 1	0.8 ± 0.3	3.0 ± 0.3
9	1998-11-22	06:42	X3.7	06:39:17–06:39:21	2.9 ± 0.1	S27 W82	ND	22/09:00	17 ± 6	0.8 ± 0.2	1.8 ± 0.2
10	1998-11-24	02:20	X1.0	02:17:47–02:22:30	2.9 ± 0.1	S30 W81	1798/1798	24/10:00	18 ± 8	0.6 ± 0.3	1.6 ± 0.1
11	2000-07-14[b]	10:24	X5.7	10:20:25–10:22:13	3.2 ± 0.1	N22 W07	1775/2061	14/18:00	45 ± 7	0.6 ± 0.3	2.2 ± 0.2
12	2000-11-08	23:28	M7.4	23:17:51–23:18:49	3.6 ± 0.2	N20 W66	1738/ND	09/15:00	40 ± 10	0.6 ± 0.2	3.0 ± 0.1
13	2000-11-25	18:50	X1.9	18:38:02–18:38:23	3.7 ± 0.1	N20 W23	671/893	26/20:00	11 ± 1	0.8 ± 0.3	2.9 ± 0.2
14	2001-04-10	05:26	X2.3	05:19:05–05:19:54	3.7 ± 0.2	S23 W09	2411/2940	11/01:00	6 ± 2	0.6 ± 0.2	2.8 ± 0.3
15	2001-10-01	05:02	M9.1	05:01:11–05:01:27	4.2 ± 0.2	S18 W80	1405/1409	01/23:00	25 ± 7	0.7 ± 0.2	4.0 ± 0.2

[b] Event associated with a ground-level enhancement (GLE)
[c] No data

3. Statistical Analysis of the Relationships between the Spectra of Proton Events and their Possible Sources

3.1. The Slope of the Proton Spectrum above the Break Energy

Attempts to correct the proton spectrum for the longitude of the solar source region did not lead to a positive result, and therefore we did not take it into account in our statistical analysis. Figure 3 presents the statistical relationship between the HXR spectral index [$\gamma_{\rm HXR}$] and the proton spectral slope above the break energy [$\gamma_{\rm p2}$]. The scatter plot shows a clear trend that looks close to linear. Uncertainties are considerable for both proton spectral indices and HXR indices. To take into account the uncertainties in both dimensions, we used two regression algorithms. One is the linear orthogonal distance regression (ODR: docs.scipy.org/doc/external/odrpack_guide.pdf). The second algorithm is the reduced major axis regression (RMA: Harper, 2016) that is implemented in the pylr2 Python package available at github.com/OceanOptics/pylr2. The correlation coefficients that we obtained using the two algorithms are the same.

The correlation coefficient between the proton index above the break energy and the HXR spectral index for both RHESSI and Yohkoh events is $\rho = 0.86$. The linear regression equation, which was also obtained for the whole data set using the ODR algorithm, is $\gamma_{\rm p2} = (1.91 \pm 0.17)\gamma_{\rm HXR} - (4.03 \pm 0.56)$, and $\gamma_{\rm p2} = (1.85 \pm 0.19)\gamma_{\rm HXR} - (3.81 \pm 0.67)$ using the RMA algorithm. Being slightly different from each other, the quantities in the regression equations coincide to within the uncertainties. The regression equation obtained from a single power-law fit of the proton spectra by Bhatt, Jain, and Awasthi (2013) as a dependence of [$\gamma_{\rm HXR}$] on [$\gamma_{\rm p}$] (also statistically significant) can be transformed to the form $\gamma_{\rm p} = (1.64 \pm 0.03)\gamma_{\rm HXR} - (1.34 \pm 0.05)$. The values of the coefficient between the proton and photon indices in these equations are comparable, but they are not obvious and need investigation. Among the possible reasons for the offset may be the difference between our usage of the photon index related to the major HXR peak and the hardest photon index during a flare that Bhatt, Jain, and Awasthi (2013) used.

The correlation coefficient between [$\gamma_{\rm p2}$] and the plane-of-the-sky CME speed is as low as -0.24 (and -0.25 for the deprojected CME speed) that does not support the statistically significant shock-related contribution to the near-Earth proton spectrum above the break energy. In this respect, our results are different from those obtained by Tripathi et al. (2013) and Bhatt, Jain, and Awasthi (2013), who used a single power-law fit of the proton spectra.

In the absence of a noticeable shock-related contribution, a significant correlation between the spectral index of the near-Earth protons above the break energy and the power-law index of the bremsstrahlung produced by flare electrons definitely indicates their common origin in the majority of events. The correspondence is reinforced by the linearity of the relationship between both spectra that is not complicated by a complex dependence on different parameters, as in the case of the gyrosynchrotron emission (Dulk and Marsh, 1982). Note also that the correlation coefficient of $\rho = 0.86$ can be somewhat reduced because of wave-particle interactions, which modify the simple relationship $\gamma = \delta - 1$

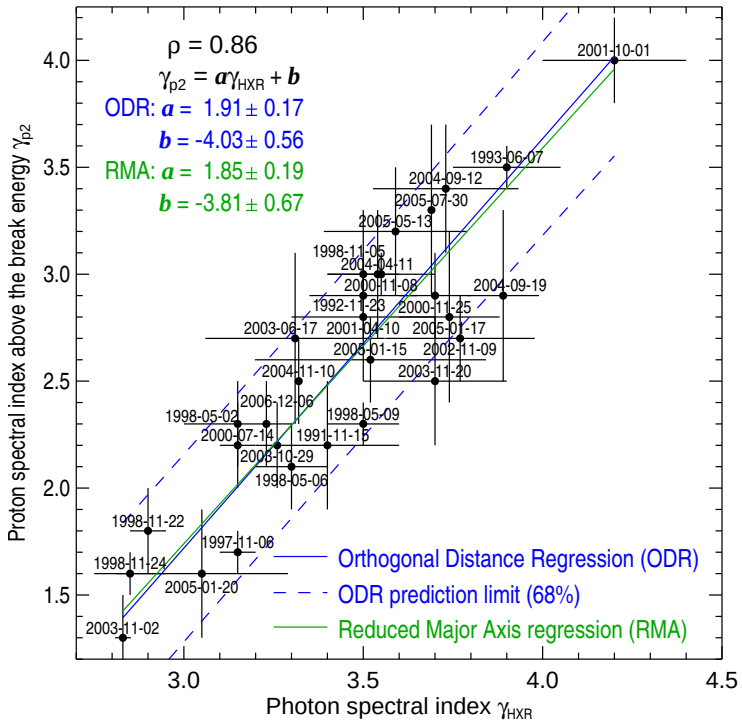

Figure 3. Scatter plot of the slope of the integral proton spectrum above the break energy versus the HXR spectral index. Uncertainties are represented by bars centered on black dots, corresponding to events whose dates are indicated alongside. The correlation coefficient specified in the upper-left corner was calculated for all 30 events. The blue line represents the linear ODR fit of the distribution and the green line represents its RMA fit. The regression coefficients obtained by the two methods are denoted by the corresponding colors. The two blue-dashed lines denote a 68 % confidence level of the best ODR fit.

between the power-law spectral index of the electron spectrum [δ] and that of bremsstrahlung [γ], which they produce via thick-target emission (Hannah and Kontar, 2011). On the other hand, the shock-related contribution to the proton spectrum above the break energy in a small number of events is not excluded.

3.2. The Slope of the Proton Spectrum below the Break Energy

Figure 4 presents the statistical relationship between the plane-of-the-sky CME speed and the proton spectral slope below the break energy [$\gamma_{\rm p1}$] for 24 out of 30 events, for which CME speeds are known. The uncertainties in the CME velocities are unknown, but they are unlikely to make a significant contribution to the statistical relationship in comparison with the large uncertainties of the proton index [$\gamma_{\rm p1}$]. The cause of the latter is a large scatter of data from different detectors used in compiling the catalogs of proton events (see, e.g., Figure 1).

Figure 4 shows a trend of anticorrelation between [$V_{\rm CME}$] and [$\gamma_{\rm p1}$]. Both ODR and RMA linear algorithms gave $\rho = -0.75$ for this relationship and even higher correlation coefficient $\rho = -0.81$ for the relationship between the deprojected

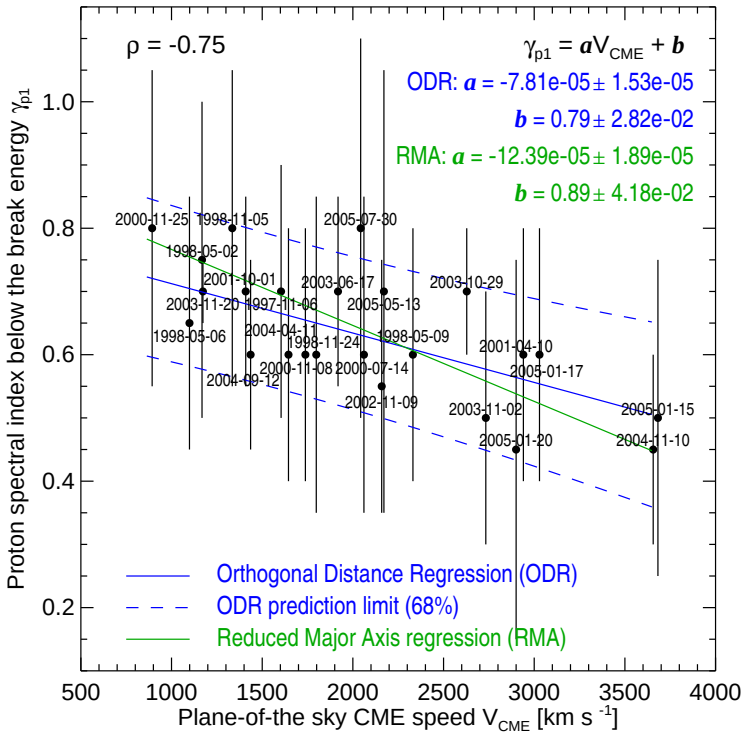

Figure 4. Scatter plot of the slope of the integral proton spectrum below the break energy [$\gamma_{\rm p1}$] versus the plane-of-the-sky CME speed [$V_{\rm CME}$]. The correlation coefficient specified in the upper-left corner was calculated for 24 events. All other notations are the same as in Figure 3.

CME speed and [$\gamma_{\rm p1}$]. On the other hand, the correlation between [$\gamma_{\rm HXR}$] and [$\gamma_{\rm p1}$] with $\rho \approx 0.16$ is insignificant. The high anticorrelation between [$V_{\rm CME}$] and [$\gamma_{\rm p1}$] indicates the predominant contribution of the shock-related acceleration of protons below the break energy; the higher the CME speed, the stronger the CME-driven shock, and the harder the spectrum of protons it accelerates.

The linear ODR fit for this data set is $\gamma_{\rm p1} = (-7.81 \pm 1.53) \times 10^{-5} V_{\rm POS\ CME} + (0.79 \pm 0.03)$ and the RMA fit is $\gamma_{\rm p1} = (-12.39 \pm 1.89) \times 10^{-5} V_{\rm POS\ CME} + (0.89 \pm 0.04)$. The regression line that the RMA algorithm issues visually seems to reflect the trends better than the ODR algorithm (Carr, 2012). Bhatt, Jain, and Awasthi (2013) obtained a stronger dependence on the CME speed of $V_{\rm CME}^{3.23}$ from a single power-law fit of the proton spectrum, whose overall slope is considerably steeper than its low-energy branch. Another difference of our results from those obtained by Tripathi et al. (2013) and Bhatt, Jain, and Awasthi (2013) is the lack of correlation between the CME speeds and the photon spectral indices, which we estimated for the HXR peaks.

Acceleration of protons by shock waves in this energy range is widely accepted. Moreover, many authors suggest that CME-driven shocks accelerate protons to higher energies. In support of this view, Li and Lee (2015) and Zhao, Zhang, and Rassoul (2016) demonstrated that the double power-law differential energy

spectra resulted from interplanetary transport effects. In particular, Li and Lee (2015) reproduced in their modeling the spectra and break energies of some events considered by Mewaldt et al. (2012), although with a smaller difference between the slopes below and above the breakpoints.

However, transport effects are unlikely to destroy the correlation between the slopes $[\gamma_{p1}]$ below the breakpoints and $[\gamma_{p2}]$ above them, and to organize a high correlation between $[\gamma_{p2}]$ and $[\gamma_{HXR}]$ in parent flares that was found in the preceding section. On the other hand, transport effects may reduce the latter correlation.

3.3. Proton Spectra at High Energies and in GLE Events

Ground-level enhancements in cosmic-ray intensity (GLEs) represent the highest-energy extremity of SEP events (e.g. Miroshnichenko, 2015; Moraal and McCracken, 2012; Bruno et al., 2018), where collisions of GeV-energy protons with Earth's neutral atmosphere produce secondary neutrons that are detected by ground-based neutron monitors (NM). Mewaldt et al. (2012) analyzed the differential energy spectra of event-integrated proton fluences in the range from ≈ 0.1 to 500–700 MeV in major SEP events associated with 16 GLEs in Solar Cycle 23. They found that all of the proton spectra exhibited spectral breaks at energies ranging from ≈ 2 MeV to about 46 MeV and that all of them were well fitted by a double power-law shape. The break energy is uncorrelated with $[\gamma_{p2}]$, while there is a high correlation ($\rho \approx 0.8$) between the break energy and $[\gamma_{p1}]$. The correlation is probably a methodical effect, as Bruno et al. (2018) showed; the best fit for a steeper power law (larger γ) is reached when the greater falloff at higher energies in the power law is compensated for by a higher rollover energy.

We analyze the time-of-maximum integral spectra of proton fluxes that are not expected to be identical to the spectra of the event-integrated proton fluences, which are not affected by the velocity dispersion and accumulate the contributions from all implicated sources. In addition, the slope of an integral spectrum is less by unity than the slope of the corresponding differential power-law spectrum. Keeping in mind these differences, we compare our results with those presented by Mewaldt et al. (2012).

In all of the proton spectra that we analyzed, the spectral break occurred at energies ranging from ≈ 3 MeV to about 63 MeV that is consistent with the result of Mewaldt et al. (2012). We compared the spectral slopes that we estimated below the break energy $[\gamma_{p1}]$ and above it $[\gamma_{p2}]$ with the corresponding slopes of the differential spectra of the proton fluences evaluated by Mewaldt et al. (2012). We found the correlation coefficient of 0.73 between the two slopes above the break energy $[\gamma_{p2}]$ and 0.66 between the two slopes below the break energy $[\gamma_{p1}]$ with a difference between the average values of the corresponding slopes around unity, as expected. The $[\gamma_{p1}]$ and $[\gamma_{p2}]$ slopes do not correlate with each other in the events considered by Mewaldt et al. (2012) and in our larger set of events as well. There is no correlation between the break energy and any of the spectral slopes we found.

We also compared parameters $[\gamma_{p1}]$, $[\gamma_{p2}]$, and E_0 observed in our sets of GLE and non-GLE events. There is a small difference in the means of $[\gamma_{p1}]$ because of

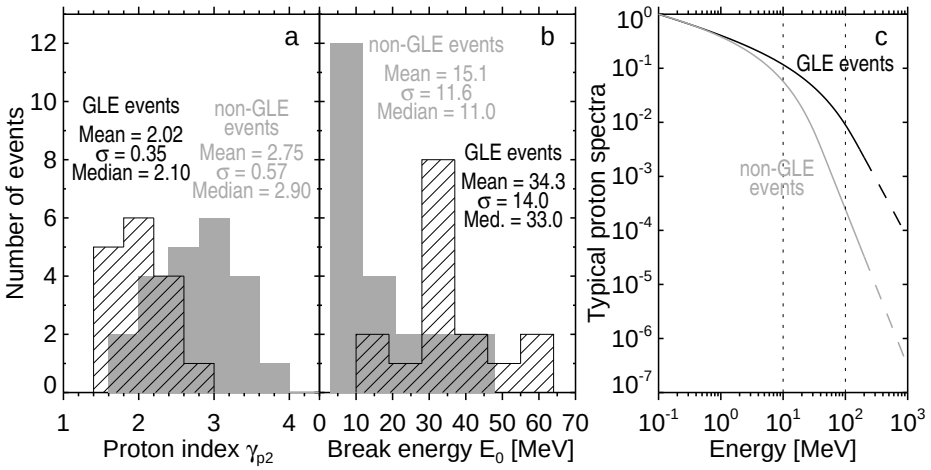

Figure 5. Distributions of the slopes of the proton spectra above the break energy γ_{p2} (**a**) and of the break energies E_0 (**b**) for 16 GLE events (black line-filled) and 22 non-GLE events (gray-shaded). **c**) Normalized time-of-maximum integral proton flux spectra for typical GLE (black) and non-GLE (gray) events from our data sets. The dashed lines extrapolate to higher energies the power-law slopes γ_{p2} above the break energies without rollovers.

three statistically insignificant outliers (events 1, 2, and 3 in Table 2), where the spectral breaks are poorly pronounced. These events are not present in Figure 4. Without the outliers, the mean $\overline{\gamma_{p1}} = 0.63 \pm 0.11$ and the median value of the low-energy slope is 0.60 for both GLE and non-GLE events.

In addition to the difference between $[\gamma_{p2}]$ in GLE and large non-GLE events found by Mewaldt et al. (2012), a difference between the break energies is manifested in our set of events of a wider range. Figure 5a presents the distributions of the higher-energy slopes γ_{p2} for the 22 non-GLE events from our set and 16 GLE events. Figure 5b shows the distributions of the break energies E_0 for these events.

The distributions of γ_{p2} as well as E_0 in GLE and non-GLE events overlap, while the two parameters do not correlate with each other. Both populations most likely represent subsets of a continuous distribution of proton events with a large scatter in the parameters of their spectra. GLE events are at the highest-energy end of this set.

Figure 5c presents schematic time-of-maximum integral proton flux spectra calculated for a typical non-GLE event from out set and for a typical GLE event. The differential spectra were represented by the Band function (Equation 2), whose input values were supplied to obtain the median values of $[\gamma_{p1}]$, $[\gamma_{p2}]$, and E_0. We set the low-energy slope $[\gamma_{p1}]$ of 1.2 for non-GLE events and 1.3 for GLE events (vs. 1.25 found by Mewaldt et al., 2012) that gave $\gamma_{p1} \approx 0.4$ in the integral spectrum at lowest energies that is close to the observed value. The spectra are normalized to unity at 0.1 MeV.

Figure 5c shows that the break energy affects the proton flux at high energies even stronger than the power-law index $[\gamma_{p2}]$. The proton flux at about 1 GeV is two orders of magnitude higher in GLE events than in non-GLE events. Probable

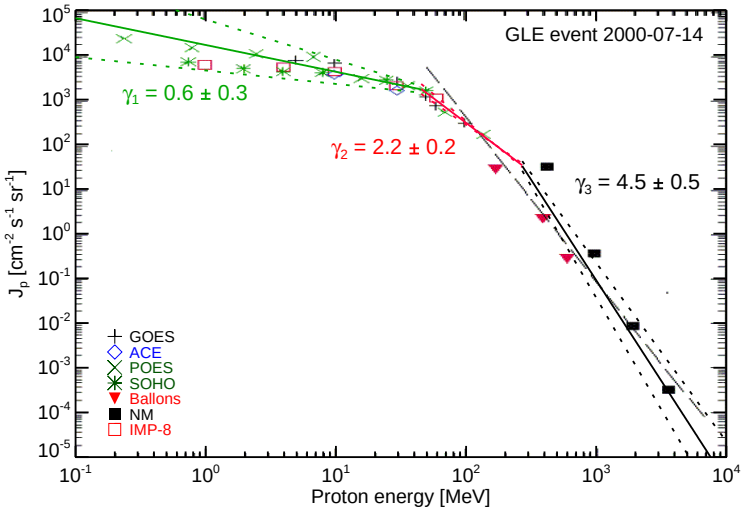

Figure 6. The time-of-maximum integral proton spectrum for the SOL2000-07-14 GLE59 event (symbols) presented in the catalog by Logachev et al. (2016) along with the solid lines that fit its three branches. The black-filled squares represent the NM data. The dotted lines represent the uncertainties in the spectral slopes.

high-energy rollovers are unlikely to reduce the difference. The figure also illustrates the difference in the hardness, $\delta_{\rm p} = \log_{10}(J_{10\,\rm max}/J_{100\,\rm max})$, between the two sets of events. Here $J_{10\,\rm max}$ and $J_{100\,\rm max}$ are the peak fluxes in the >10 MeV and >100 MeV integral proton channels. For the two typical spectra, $\delta_{\rm p} \approx 2.4$ in non-GLE events and $\delta_{\rm p} \approx 1.1$ in GLE events. If $J_{10\,\rm max}$ exceeds $J_{100\,\rm max}$ by no more than one order of magnitude in a large proton event and its solar source region is not far from the well-connected position, then a GLE is possible.

The proton spectra presented in the catalog by Logachev et al. (2016) are supplemented for GLE events by the highest-energy part reconstructed from the data of the Neutron Monitor Network. The reconstruction method is described in the catalog. In those events, where the highest-energy spectral part based on the NM data has three or more points, its slope is steeper than $[\gamma_{\rm p2}]$, as stated previously (e.g. Tylka and Dietrich, 2009). Thus, the second break in the spectrum seems to exist in GLE events between 150 and 450 MeV. An example of a full proton spectrum with two break points reconstructed for the SOL2000-07-14 GLE59 event is shown in Figure 6. Neither the second-break energy nor the spectral slope above it correlate with any of the parameters out of $[\gamma_{\rm p1}]$, $[\gamma_{\rm p2}]$, $[\gamma_{\rm HXR}]$, and $[V_{\rm CME}]$. A small number of GLEs in the catalogs we used and insufficient quality of the spectra do not allow clarifying the situation. We therefore invoke later studies of high-energy SEPs.

Bruno et al. (2018) presented detailed proton spectra measured from 80 MeV to about 1 GeV in the Payload for Antimatter–Matter Exploration and Light-nuclei Astrophysics (PAMELA) satellite experiment in SEP events that occurred in 2006–2014. The authors established that the Ellison–Ramaty spectral shape (Equation 1) matched the observed spectra and tabulated their parameters. They found no qualitative distinction between the spectral shapes in GLE and

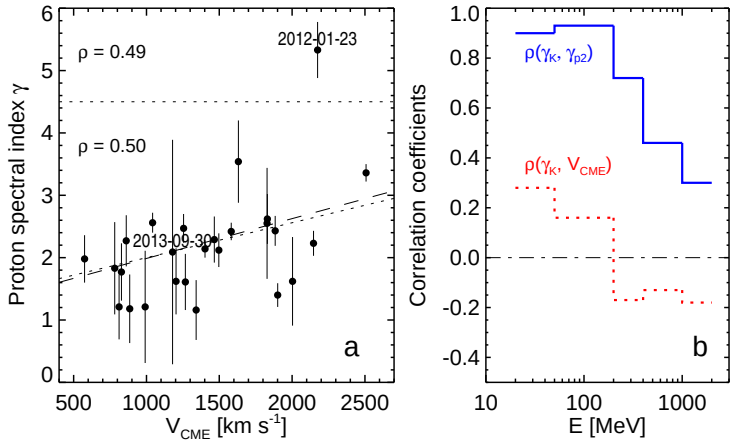

Figure 7. a) Scatter plot of the proton spectral index vs. CME speed according to data of Bruno et al. (2018). The vertical bars represent the uncertainties. The slanted lines represents the linear regression calculated for the whole data set (dashed) and without the SOL2012-01-23 outlier (dotted). The corresponding correlation coefficients are specified. **b**) Correlation coefficients between the slopes of the GLE spectra [γ_K] calculated from Koldobskiy et al. (2021) data at different energies and [γ_{p2}] evaluated by Mewaldt et al. (2012) (blue-solid) and between [γ_K] and CME speeds (red-dotted). The dash-dotted line denotes the zero level.

non-GLE events and confirmed that GLEs were the subset of a continuous distribution of SEP events, more intense at high energies. The authors also stated that while the observed spectral forms were consistent with diffusive shock acceleration theory, the relative influences on the SEP spectra of acceleration and transport processes was not clear.

The absence of a temporal overlap between the events we analyzed and the PAMELA observations does not allow its direct comparison. Instead, we consider a possible correlation between the spectral slopes evaluated by Bruno et al. (2018) for 26 SEP events and the speeds of associated CMEs plotted in Figure 7a. There is a weak correlation between the spectral slopes [γ] and V_{CME} of 0.50 for the whole data set and 0.49 without the SOL2012-01-23 outlier, whose influence is thus insignificant. The rollover energies are independent of V_{CME} ($\rho = 0.015$). It is important that the correlation with V_{CME} is positive, whereas it would have to be negative, if CME-driven shocks were responsible for the acceleration of protons observed by PAMELA (cf. Figure 4). This circumstance supports the Bruno et al. (2018) idea that the observed spectral shape is determined by transport effects and not by the acceleration process.

While the break energies found by Mewaldt et al. (2012) and in our events range from units to tens of MeV, the rollover energies found by Bruno et al. (2018) are higher, with a mean of 171 MeV. The difference indicates that the rollovers detected in the PAMELA data probably represent the second inflection point in most proton spectra. The SOL2013-09-30 non-flare-associated event denoted in Figure 7a is probably one of the few exceptions, whose overall spectral shape matches the Ellison–Ramaty pattern. Its rollover energy of 42 ± 24 MeV is the lowest among the PAMELA events and falls into the range of the break

energies that we found. This SEP event was most likely of a purely shock-accelerated origin (Gopalswamy et al., 2015; Cliver et al., 2019; Grechnev and Kuzmenko, 2020).

To get a conception of the overall proton spectrum, we involve the study by Koldobskiy et al. (2021), who presented the results of a full revision of the spectral fluences for most GLE events that occurred in 1956–2017. The authors fitted the measured data versus rigidity with a modified Band function (Equation 2 supplemented with the second, highest-energy rollover), and tabulated the results. The spectra presented by Koldobskiy et al. (2021) and Bruno et al. (2018) for the only overlapping SOL2012-05-17 GLE71 event agree well with each other. Generally, the 30 GLE spectra reconstructed by Koldobskiy et al. (2021) in a range corresponding to energies from about 20 MeV to GeVs are more complex than the Ellison–Ramaty pattern.

Using the Koldobskiy et al. (2021) parametrization and tabulated values, we transformed the integral rigidity spectra into differential energy spectra and estimated their slopes $[\gamma_{\rm K}(E)]$ within five energy intervals bounded by 20, 50, 200, 400, 1000, and 2000 MeV for 14 GLEs, which overlap with the events that Mewaldt et al. (2012) and we analyzed. Direct comparison of $[\gamma_{\rm K}(E)]$ with $[\gamma_{\rm HXR}]$ was inconclusive, because only six out of eight GLE events listed in our Tables 1 and 2 are present in the Koldobskiy et al. (2021) catalog.

Instead, in Figure 7b we compare $[\gamma_{\rm K}(E)]$ with the slope $[\gamma_{\rm p2}]$ above the break energy evaluated by Mewaldt et al. (2012), keeping in mind a high correlation between $[\gamma_{\rm p2}]$ and $[\gamma_{\rm HXR}]$ established in Section 3.1. The correlation is highest ($\rho = 0.93$) in the 50–200 MeV energy range in agreement with our result and decreases with increasing energy, similar to what we observed for the GLE spectra in the Logachev et al. (2016) catalog. The correlation between $[\gamma_{\rm K}(E)]$ in adjacent energy intervals is high; Cliver et al. (2020) also demonstrated a high correlation between > 200 MeV and > 430 MeV proton fluence. The correlation between $[\gamma_{\rm K}(E)]$ and CME speeds is insignificant in all energy intervals.

By combining the parametrization and input quantities tabulated by Koldobskiy et al. (2021) with those presented by Mewaldt et al. (2012), it is possible to reconstruct proton fluence energy spectra in the whole energy range. Figure 8 shows an example calculated for the SOL2000-07-14 GLE59 event. The two parts were concatenated at an energy of 37 MeV, where their shapes and slopes matched best. The discrepancy of 2.08 was compensated for by multiplying one part and dividing another part by a factor of 1.44. Note that i) the result of a parametrization is an approximation of a real spectrum and may not reproduce its details accurately, ii) the parametrization input values may differ slightly from the resulting characteristics, and iii) the spectra in Figure 8 at energies > 37 MeV are determined by Koldobskiy et al. (2021) parametrization and may differ from Mewaldt et al. (2012) results. The parts of the energy spectra calculated from the Koldobskiy et al. (2021) data get steeper with increasing energy without pronounced breaks. The slopes of the differential fluence spectrum indicated in Figure 8a ($\gamma_{\rm p1} = 1.24$, $\gamma_{\rm p2} = 3.24$) do not exactly match the values that Mewaldt et al. (2012) found ($\gamma_{\rm p1} = 1.09 \pm 0.03$, $\gamma_{\rm p2} = 3.80 \pm 010$), being not much different from them. Comparison of the integral fluence spectrum in Figure 8b with the

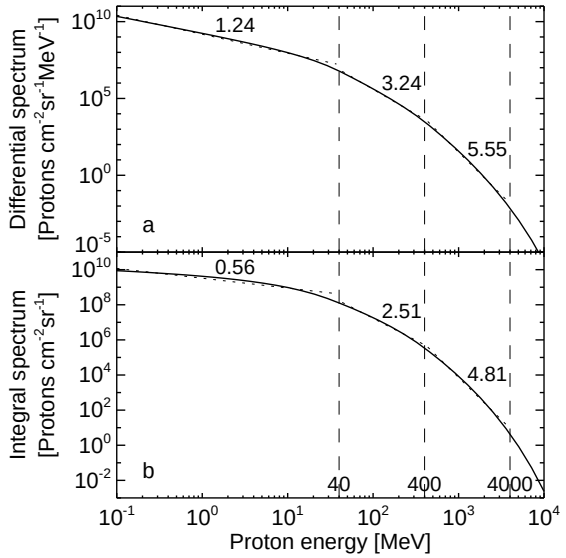

Figure 8. Synthetic differential (**a**) and integral (**b**) event-integrated proton fluence energy spectra reconstructed for the SOL2000-07-14 GLE59 event (cf. Figure 6) using the parametrization of Mewaldt et al. (2012) and that of Koldobskiy et al. (2021). The slanted thin-dotted lines represent the slopes indicated within the energy intervals bounded by the vertical dashed lines.

time-of-maximum integral flux spectrum from the Logachev et al. (2016) catalog in Figure 6 shows a similar relationship.

In summary, considerations of the Bruno et al. (2018) and Koldobskiy et al. (2021) results confirm the outcome from the analysis of the Logachev et al. (2016) catalog. The contribution of CME-driven shocks dominates at low proton energies and does not appear statistically at higher energies. The flare-related contribution dominates at proton energies from several tens of MeV up to about 400 MeV. The slope of the proton spectrum at higher energies does not show a statistically significant correlation with either the HXR emission spectrum or the CME speed, possibly due to transport effects.

4. Discussion

The results of our statistical analysis allow identifying the two components in the proton spectra; the shock-related contribution dominates at the proton energies roughly below 50 MeV, while the flare-related contribution dominates at higher proton energies up to several hundred MeV. This outcome corresponds to the conclusions by Klein and Trottet (2001), Dierckxsens et al. (2015), Trottet et al. (2015), and Papaioannou et al. (2016).

We expected these statistical relationships, considering the flux-rope-mediated transport scenario of flare-accelerated particles until their release in reconnection with an open structure (Masson, Antiochos, and DeVore, 2013; Kocharov et al., 2017; Grechnev et al., 2017a). The presence in an expanding flux rope of trapped

electrons as probable tracers of protons can be revealed by a drifting Type IV burst and their release is marked by a decametric/hectometric (DH) Type III burst (Grechnev et al., 2017a, 2019). Flare-accelerated electrons and protons trapped in the flux-rope magnetic structure experience Coulomb collisions with its dense plasma. From the analogy with the processes that affect electrons in a static trap one might expect a progressive depletion of the low-energy parts of the electron and proton spectra after an impulsive injection into the trap (see, e.g., Figure 3 in Metcalf and Alexander, 1999). The processes in an erupting flux rope are complicated by its rapid expansion, so that adequate investigation is necessary to comprehend them. Nevertheless, some analogy with a static trap seems to hold.

Rapid energy losses by numerous lower-energy electrons are supported by the indications of the collisional heating of erupting flux ropes by injected flare-accelerated electrons (Glesener et al., 2013; Grechnev et al., 2019). As shown by Grechnev et al. (2017a), the flux-rope-mediated scenario sheds also light on the large excess of the electron-to-proton ratios (e.g. 0.5 MeV electrons to >100 MeV protons) observed in gradual events over their values in impulsive events that Cliver (2016) and Cliver et al. (2019) emphasized. The lifetime of 100 MeV protons exceeds the lifetime of 0.5 MeV electrons in plasma of the same density $[n]$ by two orders of magnitude. Thus, the electron-to-proton ratio for particles that escape from a flux rope with an initial density $n > 10^{10}\,\mathrm{cm}^{-3}$ in a gradual event may be much less than in an impulsive event, where particles escape directly from the flare site. The escape of trapped particles in reconnection of the expanding flux rope with an open structure is supported by the correspondence of the proton release time estimated by Reames (2009) for several GLE events to the onset of DH Type III bursts that was found by Grechnev et al. (2017a).

While the flux-rope-mediated scenario gets support from several observational facts, this scenario along with other recent conclusions considerably changes the expectations from traditional assumptions. For example, flare-accelerated particles escape in this scenario relatively high in the corona, at a flank of a CME where its flux rope reconnects with an open structure, and not directly from the flare site. This circumstance calls for rethinking conclusions made without considering such a possibility (e.g. Tan et al., 2013; Cliver et al., 2020).

On the other hand, shock waves most likely appear in all solar eruptive events that produce SEPs, even if the event is non-flare-related (e.g. the SOL2013-09-30 event mentioned in Section 3.3; Gopalswamy et al., 2015). As recent studies found in all analyzed events, a shock wave develops as a piston-shock, which is impulsively excited by an abruptly expanding structure such as an eruptive filament. The piston-shock initially resembles a hypothetical flare-generated decelerating blast wave (e.g. Grechnev et al., 2011, 2018; Uralov, Grechnev, and Ivanukin, 2019). If the CME is fast, then the piston-shock gradually changes to the bow shock, whose speed corresponds to the CME speed. Otherwise, if the CME is slow or absent, then the piston-shock decays into a weak disturbance soon. This circumstance explains a low proton yield of the events accompanied by metric but not by DH Type IIs (Cliver, Kahler, and Reames, 2004) or those associated with slow CMEs.

In the case of a fast CME, the persistently driven bow shock accelerates protons for a long time, progressively elevating their spectrum to higher energies. The highest energy acquired by shock-accelerated protons is probably determined by specific conditions in particular events; the response was observed in the > 100 MeV GOES channel in some non-flare-related proton events (e.g. Gopalswamy et al., 2015; Grechnev and Kuzmenko, 2020). The high efficiency of the Fermi process operating herewith also ensures the acceleration of heavier ions high in the corona that governs their properties observed in gradual events.

Thus, the results of our analysis as well as the conclusions drawn in different recent studies indicate that near-Earth proton enhancements produced by flare-related solar events are a combination of both shock-accelerated and flare-accelerated contributions with a statistical predominance of the former at the lower energies and the latter at the higher energies. Hence, the bulk of GeV-energy protons responsible for GLE events is most likely accelerated by flare processes in the majority of GLEs, although the shock-acceleration appears to be entirely responsible for exceptional GLE events (Cliver, 2006).

Vashenyuk et al. (2008), McCracken, Moraal, and Stoker (2008), and Moraal and McCracken (2012) revealed in some GLEs impulsive and gradual components with different temporal profiles, anisotropy, and spectra. They proposed that the high-energy impulsive component was due to flare processes, whereas Cliver et al. (2020) advocated its shock-related origin. Some authors associated the delayed gradual component with CME-driven shock waves, while Vashenyuk et al. (2008) related its source to flare processes of a different kind than those responsible for the impulsive component. Klein (2021) supported the latter view, pointing to Type IV bursts as a manifestation of a post-impulsive time-extended acceleration in the wake of a CME.

Our results are unlikely to bring final clarity to this controversy. A direct comparison of the HXR spectral slopes with those of near-Earth proton spectra and with CME speeds indicates the predominance of the flare-acceleration at proton energies up to about 200 MeV. An indirect comparison with the data of Bruno et al. (2018) and Koldobskiy et al. (2021) extends this conclusion to 400 MeV. The shock-acceleration does not show up statistically at energies of tens to hundreds of MeV.

The highest-energy part of the proton spectra reconstructed in GLE events from the NM data is steeper than the spectral slope $[\gamma_{p2}]$ in the energy range of 50–200 MeV. The highest-energy slope does not correlate with $[\gamma_{p2}]$, the HXR photon index, or the CME speed. It is highly unlikely that protons are accelerated to relativistic energies by anything other than flares and shock waves. Implication of transport effects is possible, as Bruno et al. (2018) assumed. An impression appears of some kind of "cooling" of relativistic protons trapped in the expanding flux rope. However, the cooling effect close to the Sun in a flux rope, whose ends are rooted to the solar surface, seems to be questionable. Elucidation of the reason for the lack of correlation between the highest-energy spectral slope in GLE events and the parameters of their possible solar sources requires further analysis.

5. Summary

Based on the scenario of the flux-mediated transport of flare-accelerated protons in an erupting flux rope, we have studied possible relationships between the time-of-maximum spectra of near-Earth proton enhancements observed in 1991–2006, on the one hand, and photon indices of associated HXR bursts observed by Yohkoh in 15 events and by RHESSI in 15 events and CME speeds, on the other hand. The essence of our study was to analyze separately the low-energy and higher-energy slopes of the proton spectra. The critical points in our analysis were a strict selection of well-observed flares and the choice of the strongest and hardest HXR peak for the estimation of the photon index.

The results appear to have made it possible to identify the flare-related and shock-related contributions in the proton spectra. Most likely, both CME-associated shock waves and flare processes contribute to particle acceleration in gradual SEP events. The shock-acceleration statistically dominates at the lower proton energies (roughly below 50 MeV) and the flare-acceleration statistically dominates at the higher energies (roughly between 50 and 400 MeV), although exceptions probably exist. Consistency of the results that were obtained using a number of independent data sources and different processing methods supports the reliability of the conclusions. However, the spectral indices of relativistic protons in GLE events do not correlate with either the HXR spectral indices or the CME speeds for an unclear reason possibly related to transport effects that requires further analysis.

The overall shape of an SEP spectrum is generally complex, being determined by different acceleration mechanisms and probably influenced by transport effects. The lowest-energy part (roughly < 50 MeV) is close to the Ellison–Ramaty spectral pattern of a power-law with an exponential rollover. The higher-energy part (roughly 50–200 MeV) is a steeper power-law. The highest-energy part (roughly > 200 MeV), which is observed in GLE events, possesses the second rollover that may be due to transport effects. Portions of these parts also resemble the Ellison–Ramaty pattern.

The presence of two different accelerators determines mixed properties of SEPs that complicates the identification of their sources and makes attempts to find their only origin from the analysis of particular SEP properties unsuccessful. On the other hand, the dual nature of gradual SEPs promises reconciling the apparent contradictions between different observational conclusions and conflicting views on the origin of SEPs.

A similar analysis for subsequent events seems to be promising. It is possible that a more detailed examination of the proton fluences can provide more information. The statistical relationships between the CME speeds and the shock-accelerated proton population can be refined by analyzing the extensive CDAW CME catalog and the spectra of near-Earth proton enhancements in the low-energy range, for example < 40 MeV. The flux-rope-mediated proton transport scenario also appears to deserve attention for in-depth studies. We hope that our results would help to reconcile seemingly conflicting conclusions of different studies of SEPs and to approach understanding their origins.

Acknowledgments We are grateful to K.-L. Klein for his initial idea of the CME-facilitated escape of flare-accelerated protons, whose elaboration inspired this study, and to A.A. Kochanov and A.M. Uralov for useful discussions. We are indebted to the anonymous reviewer for valuable remarks and suggestions. We thank the teams that operated RHESSI and Yohkoh. Yohkoh was a mission of ISAS in Japan, with contributions from the US and UK. We thank the authors of the catalogs of proton events and Yohkoh observations for the data used here and the team maintaining the CME Catalogs at the CDAW Data Center by NASA and the Catholic University of America in cooperation with the Naval Research Laboratory. SOHO is a project of international cooperation between ESA and NASA. We also thank the Konus-Wind team at the Ioffe Institute.

The statement of the problem, analysis of statistical relationships between the spectra of proton events and their solar sources, and discussion of the results was funded by the Russian Science Foundation under grant No. 21-72-00039 (V. Kiselev; Sections 1, 2.1, 3, and 4). Processing and analysis of hard X-ray data (N. Meshalkina; Section 2.2) and selection of events (V. Grechnev; Sections 2.3, 3.3, and Appendix) were financially supported by the Ministry of Science and Higher Education of the Russian Federation.

Data Availability

All data generated or analyzed during this study are included in this published article.

Disclosure of Potential Conflicts of Interest

The authors declare that they have no conflicts of interest.

Appendix

A. Excluded events

The catalogs of solar proton events composed by Logachev et al. (2016) and by Sladkova et al. (1998) contain information about probable solar sources of the near-Earth proton enhancements that is certain for the majority of events. Nevertheless, identification of some events is ambiguous. We checked these events using the online CDAW CME catalog (Yashiro et al., 2004: cdaw.gsfc.nasa.gov/CME_list/), the online RHESSI browser at sprg.ssl.berkeley.edu/~tohban/browser/?show=qli, the Yohkoh catalog composed by Sato et al. (2006) that is available in the electronic form at dx.doi.org/10.1007/s11207-006-1831-5, the Yohkoh resident database of the SolarSoft as well as other sources of information on solar events. The events with a questionable flare association were filtered out.

A number of events were excluded, because their parent flares occurred during the night of RHESSI or Yohkoh or when they passed in the South-Atlantic Anomaly (SAA), where the observations were interrupted. An example that is not obvious is the SOL2006-12-13 GLE70 event (No. 46 in Table 3); almost the whole flare duration was observed by RHESSI, but the first HXR peak at 02:25, which was the strongest and hardest, was missed because of RHESSI night (Grechnev et al., 2013a). On the contrary, the Konus-Wind data terminated just before the main peak. An attempt to use the RHESSI spectrum for the second

major peak at 02:29, which was recorded also incompletely, resulted in an outlier in the scatter plot in Figure 3. We therefore were forced to exclude this event. Another reason for the exclusion of an event was the flare location behind the limb (e.g. the SOL2001-04-18 GLE61 event, No. 14 in Table 4).

As mentioned in Section 2, we applied the condition $2.5 < \gamma_{\mathrm{HXR}} < 4.5$. This criterion was chosen rather arbitrarily and was confirmed in the course of the analysis. We assumed that a still softer photon index indicated meager acceleration processes, which were unlikely to provide a significant $> 50\,\mathrm{MeV}$ proton yield of our interest. On the other hand, a super-hard photon index does not seem realistic. In all cases when γ_{HXR} did not fit into this range, the cause was identified. We refined the time of the HXR peak in some events. As Tables 3 and 4 show, additional reasons were revealed to exclude other events with a questionable photon index, e.g. incomplete flare observations, probable data issues, etc. The situation with $\gamma_{\mathrm{HXR}} > 4.5$ along with a flare location very close to the limb indicated that the flare site could be partly occulted, which is also unacceptable.

Some events still were outliers on scatter plots. We examined each of them and identified the cause. In some cases, the spectra were non-monotonic and had a hump. Multiple changes of the operational mode occurred during some observations, as in the SOL2006-12-14 event (No. 47 in Table 3). For some questionable events, neither quick-look spectra nor quick-look images are present at the RHESSI browser. We rated all of these cases as data issues.

Table 3 presents the complete list of 47 RHESSI events excluded from the analysis. Table 4 presents a similar list of 17 excluded Yohkoh events.

Table 3. Events excluded from the analysis (RHESSI data).

No.	Solar flare						$V_{\rm CME}$	Near-Earth protons		
	Date	GOES		RHESSI	$\gamma_{\rm HXR}$	Position	POS/rad	Peak	E_0	$\gamma_{\rm p}$
		peak	class	peak			[km s^{-1}]	[day/time]	[MeV]	
1[a]	2002-02-20	06:12	M5.1	ND	ND	N12 W72	952/965	20/08:00	16 ± 4	2.5
2[a]	2002-03-15	23:12	M2.2	ND	ND	S08 W03	957/1297	16/13:00	6 ± 2	2.7
3[a]	2002-03-18	02:30	M1.0	ND	ND	S09 E47	989/1223	18/18:15	5 ± 2	2.7
4[b,c,d]	2002-03-22	11:06	M1.6	10:58:47	4.57	S10 W90	1750/1750	22/20:00	ND	3.7
5[a]	2002-04-17	08:06	M2.6	08:15:34	3.14	S14 W36	1240/1417	17/16:00	6 ± 1	2.8
6[a,d]	2002-04-21	01:50	X1.5	02:08:38	2.86	S14 W84	2393/2396	21/03:00	ND	1.9
7[a]	2002-05-22	03:50	C5.0	03:17:34	ND	S20 W84	1557/1718	23/10:00	8 ± 2	3.8
8[a]	2002-07-07	11:30	M1.0	11:15:34	3.70	S17 W90	1423/ND	07/20:00	13 ± 3	2.8
9[a]	2002-07-15	20:06	X3.0	ND	7.30	N19 W01	1151/1453	16/22:00	12 ± 3	3.5
10[a]	2002-07-18	07:44	X1.8	ND	ND	N19 W33	1099/1265	19/11:00	4 ± 1	2.2
11[b,d]	2002-07-20	21:30	X3.3	21:34:43	6.19	S13 E90	1941/1941	22/11:00	ND	2.6
12[a]	2002-08-14	02:06	M2.3	ND	5.64	N10 W54	1309/ND	14/09:00	5 ± 1	2.5
13[c,e]	2002-08-16	12:30	M5.2	ND	ND	S14 E20	1585/1937	17/10:00	ND	2.6
14[a]	2002-08-18	21:27	M2.2	21:50:33	8.67	S10 W20	682/ND	19/03:00	6 ± 1	2.1
15[b,c]	2002-08-22	02:00	M5.4	01:53:00	4.33	S07 W62	998/1034	22/05:00	14 ± 5	1.5
16[a]	2002-08-24	01:15	X3.1	ND	8.33	S02 W81	1913/1920	24/03:00	40 ± 10	2.1
17[a]	2002-09-05	17:06	C5.2	ND	ND	N12 E28	1748/2074	06/14:00	15 ± 5	2.2
18[a]	2003-05-27	23:07	X1.3	23:05:29	3.88	S06 W20	964/1222	28/11:00	5 ± 1	2.2
19[a]	2003-05-31	02:23	M9.3	ND	ND	S07 W65	1835/1888	31/06:00	4 ± 1	1.5
20[a]	2003-10-26	06:54	X1.3	ND	6.80	S15 E31	1371/ND	26/20:00	12 ± 6	3.1

Table 3. (*Continued*)

No.	Solar flare						V_{CME}	Near-Earth protons		
	Date	GOES peak	GOES class	RHESSI peak	γ_{HXR}	Position	POS/rad [km s^{-1}]	Peak [day/time]	E_0 [MeV]	γ_p
21[c]	2003-10-26	18:06	X1.2	ND	ND	N02 W38	1537/ND	27/02:00	20 ± 5	2.9
22[a]	2003-10-28	11:07	>X17	11:14:00	ND	S16 E08	2459/3128	28/18:00	64 ± 14	2.9
23[a]	2003-11-04	19:50	>X17	ND	7.49	S19 W83	2657/2662	05/07:00	20 ± 4	2.7
24[a]	2003-11-20	07:47	M9.6	ND	ND	N01 W08	669/1173	20/11:00	4 ± 1	2.2
25[a,d]	2003-12-02	09:50	C7.2	09:45:50	ND	S19 W90	1393/ND	02/18:00	ND	4.0
26[c]	2004-07-22	00:30	M9.1	00:29:08	ND	N06 E25	492/ND	22/20:00	4 ± 1	2.0
27[a]	2004-07-25	15:14	M1.1	ND	ND	N08 W33	1333/1544	25/21:00	28 ± 3	2.8
28[a,d]	2004-07-31	06:57	C8.4	ND	2.28	N02 W90	259/ND	01/21:00	ND	2.3
29[b,e]	2004-11-01	03:45	M1.1	03:19:54	6.40	N15 W41	459/ND	01/08:00	ND	1.9
30[a,b,c]	2004-11-07	16:05	X2.0	16:05:49	7.48	N10 W15	1759/2218	07/23:00	6 ± 1	3.0
31[a]	2004-11-08	15:45	M2.3	ND	ND	N08 W36	605/ND	09/00:00	4 ± 1	3.2
32[b,d]	2004-11-09	17:09	M8.9	17:03:58	4.95	N07 W51	2000/2144	10/10:00	ND	2.2
33[b,c]	2005-01-15	06:30	M8.6	06:27:06	2.70	N11 E06	2049/3682	15/11:00	9 ± 1	1.7
34[b,d]	2005-06-16	20:20	M4.0	20:06:28	1.70	N09 W87	ND/ND	17/04:00	ND	1.8
35[a]	2005-07-09	22:05	M2.8	ND	ND	N11 W27	1540/1818	10/05:00	14 ± 3	1.9
36[a]	2005-07-13	14:49	M5.0	14:29:33	7.30	N10 W80	1423/1423	14/04:00	4 ± 1	2.6
37[a,d]	2005-07-14	10:54	X1.2	10:26:02	5.35	N11 W90	2115/2115	15/03:00	ND	3.2
38[a,d]	2005-07-17	ND	ND	ND	ND	> W90	1527/1527	17/18:00	ND	2.3
39[a,d]	2005-07-25	ND	ND	ND	ND	> E90	1660/1660	28/14:00	ND	2.8
40[a]	2005-08-22	01:33	M2.6	ND	ND	S09 W48	1194/1265	22/07:00	5 ± 1	2.4

Table 3. (*Continued*)

No.	Solar flare						$V_{\rm CME}$	Near-Earth protons		
	Date	GOES peak	GOES class	RHESSI peak	$\gamma_{\rm HXR}$	Position	POS/rad [km s^{-1}]	Peak [day/time]	E_0 [MeV]	$\gamma_{\rm p}$
41[a]	2005-08-22	17:30	M5.6	ND	ND	S12 W60	2378/2445	23/02:00	13 ± 2	3.1
42[a]	2005-09-07	17:44	X17	ND	ND	S06 E89	ND/ND	08/20:00	27 ± 4	2.3
43[a]	2005-09-09	20:00	X6.2	ND	ND	S12 E67	2257/2311	10/11:00	43 ± 7	3.0
44[a]	2005-09-13	19:27	X1.5	ND	ND	S09 E10	1866/2445	14/15:00	10 ± 1	3.5
45[a]	2006-12-05	10:36	X9.0	ND	4.16	S07 E79	ND/ND	05/20:00	21 ± 6	1.8
46[a,b,c]	2006-12-13	02:36	X3.4	02:29:14	3.85	S06 W24	1774/2184	13/09:00	73 ± 20	4.7
47[b,c]	2006-12-14	22:10	X1.5	22:08:04	4.28	S06 W46	1042/1139	15/00:00	19 ± 4	2.5

[a] The main flare phase is missed because of RHESSI night or SAA
[b] The spectral index in hard X-rays is out of range
[c] RHESSI data issues
[d] Event behind the limb or possibly partially occulted
[e] Questionable flare association.

Table 4. Events excluded from the analysis (Yohkoh data).

No.	Solar flare						$V_{\rm CME}$	Near-Earth protons		
	Date	GOES		Yohkoh	$\gamma_{\rm HXR}$	Position	POS/rad	Peak	E_0	$\gamma_{\rm p}$
		peak	class	measured interval			[km s^{-1}]	[day/time]	[MeV]	
1[a]	1991-10-27	05:48	X6.1	05:39:39–05:39:54	4.0	S13 E15	ND	28/14:00	ND	3.8
2[b]	1992-05-08	15:46	M7.4	15:49:37–15:53:33	3.5	S26 E08	ND	09/09:00	ND	4.3
3[b]	1992-10-30	18:16	X1.7	17:30:27–17:31:28	2.7	S22 W61	ND	31/02:00	30 ± 5	2.8
4[b]	1992-11-02	03:10	X9.0	02:59:48–03:00:30	3.0	S23 W90	ND	02/06:00	40 ± 10	1.3
5[b]	1993-03-12	18:15	M7.0	18:01:13–18:01:31	4.2	S03 W48	ND	12/21:00	ND	1.4
6[c]	1993-05-14	22:07	M4.4	22:04:27–22:05:17	4.9	N20 W48	ND	15/02:00	ND	2.0
7[c]	1998-11-07	11:06	M2.4	11:05:51–11:05:57	4.5	N14 W43	632/733	07/14:00	ND	2.4
8[b]	2000-06-10	17:02	M5.2	16:52:43–16:53:25	3.7	N22 W39	1108/1228	10/20:00	15 ± 3	2.2
9[c]	2000-06-17	02:37	M3.5	02:31:00–02:31:22	3.2	N22 W72	857/ND	18/06:00	4 ± 1	2.1
10[b]	2001-04-02	21:51	X20.0	21:35:36–21:35:39	4.5	N19 W90	2505/ND	03/07:00	25 ± 5	2.9
11[c]	2001-04-09	15:34	M7.9	15:23:54–15:25:01	3.7	S21 W04	1192/1482	09/20:00	38 ± 10	1.5
12[a,b]	2001-04-12	10:28	X2.0	10:16:31–10:17:47	3.9	S20 W42	1184/1294	12/17:00	ND	1.6
13[c]	2001-04-15	13:50	X14.4	13:50:06–13:50:54	4.4	S20 W84	1199/ND	15/16:00	15 ± 5	4.2
14[d]	2001-04-18	02:14	C2.2	02:14:28–02:15:04	4.2	S20 W90	2465/2465	18/10:00	ND	1.5
15[e]	2001-04-26	13:20	M7.8	13:09:29–13:09:51	4.2	N17 W31	1006/1257	28/05:00	4 ± 1	3.6
16[d]	2001-05-20	06:03	M6.4	06:02:17–06:02:23	3.7	S18 W90	546/ND	20/10:00	ND	1.8
17[b,f]	2001-10-22	17:59	X1.2	17:50:41–17:50:49	4.5	S18 E16	618/ND	22/21:00	4 ± 1	1.5

[a] Questionable proton spectrum data
[b] The main flare phase is missed because of Yohkoh night or SAA
[c] Yohkoh data issues
[d] Event behind the limb or possibly partially occulted
[e] Questionable flare association
[f] The spectral index in hard X-rays is out of range

References

Ackermann, M., Ajello, M., Albert, A., Allafort, A., Baldini, L., Barbiellini, G., Bastieri, D., Bechtol, K., Bellazzini, R., Bissaldi, E., *et al.*: 2014, High-energy gamma-ray emission from solar flares: Summary of Fermi Large Area Telescope detections and analysis of two M-class flares. *Astrophys. J.* **787**, 15. DOI. ADS.

Ajello, M., Baldini, L., Bastieri, D., Bellazzini, R., Berretta, A., Bissaldi, E., Blandford, R.D., Bonino, R., Bruel, P., Buson, S., *et al.*: 2021, First Fermi-LAT solar flare catalog. *Astrophys. J. Suppl. Ser.* **252**, 13. DOI. ADS.

Akinian, S.T., Alibegov, M.M., Kozlovskii, V.D., Chertok, I.M.: 1978, On quantitative diagnostics of proton bursts from characteristics of microwave radio bursts at ≈9 GHz frequency. *Geomag. Aeron.* **18**, 410. ADS.

Aptekar, R.L., Frederiks, D.D., Golenetskii, S.V., Ilynskii, V.N., Mazets, E.P., Panov, V.N., Sokolova, Z.J., Terekhov, M.M., Sheshin, L.O., Cline, T.L., Stilwell, D.E.: 1995, Konus-W gamma-ray burst experiment for the GGS Wind spacecraft. *Space Sci. Rev.* **71**, 265. DOI. ADS.

Aschwanden, M.J.: 2012, GeV particle acceleration in solar flares and ground level enhancement (GLE) events. *Space Sci. Rev.* **171**, 3. DOI. ADS.

Band, D., Matteson, J., Ford, L., Schaefer, B., Palmer, D., Teegarden, B., Cline, T., Briggs, M., Paciesas, W., Pendleton, G., Fishman, G., Kouveliotou, C., Meegan, C., Wilson, R., Lestrade, P.: 1993, BATSE observations of gamma-ray burst spectra. I. Spectral diversity. *Astrophys. J.* **413**, 281. DOI. ADS.

Bhatt, N.J., Jain, R., Awasthi, A.K.: 2013, The energetic relationship among geoeffective solar flares, associated CMEs and SEPs. *Res. Astron. Astrophys.* **13**, 978. DOI. ADS.

Brueckner, G.E., Howard, R.A., Koomen, M.J., Korendyke, C.M., Michels, D.J., Moses, J.D., Socker, D.G., Dere, K.P., Lamy, P.L., Llebaria, A., *et al.*: 1995, The Large Angle Spectroscopic Coronagraph (LASCO). *Solar Phys.* **162**, 357. DOI. ADS.

Bruno, A., Bazilevskaya, G.A., Boezio, M., Christian, E.R., de Nolfo, G.A., Martucci, M., Merge', M., Mikhailov, V.V., Munini, R., Richardson, I.G., *et al.*: 2018, Solar energetic particle events observed by the PAMELA mission. *Astrophys. J.* **862**, 97. DOI. ADS.

Carr, J.R.: 2012, Orthogonal regression: a teaching perspective. *Internat. J. Math. Edu. Sc. Techn.* **43**, 134. DOI. ADS.

Castelli, J.P., Barron, W.R.: 1977, A catalog of solar radio bursts 1966-1976 having spectral characteristics predictive of proton activity. *J. Geophys. Res.* **82**, 1275. DOI. ADS.

Chertok, I.M.: 1990, On the correlation between the solar gamma-ray line emission, radio bursts and proton fluxes in the interplanetary space. *Astron. Nachr.* **311**, 379. DOI. ADS.

Chertok, I.M., Grechnev, V.V., Meshalkina, N.S.: 2009, On the correlation between spectra of solar microwave bursts and proton fluxes near the Earth. *Astron. Rep.* **53**, 1059. DOI. ADS.

Chupp, E.L., Ryan, J.M.: 2009, High energy neutron and pion-decay gamma-ray emissions from solar flares. *Res. Astron. Astrophys.* **9**, 11. DOI. ADS.

Cliver, E.W.: 2006, The unusual relativistic solar proton events of 1979 August 21 and 1981 May 10. *Astrophys. J.* **639**, 1206. DOI. ADS.

Cliver, E.W.: 2016, Flare vs. shock acceleration of high-energy protons in solar energetic particle events. *Astrophys. J.* **832**, 128. DOI. ADS.

Cliver, E.W., Kahler, S.W., Reames, D.V.: 2004, Coronal shocks and solar energetic proton events. *Astrophys. J.* **605**, 902. DOI. ADS.

Cliver, E.W., Forrest, D.J., Cane, H.V., Reames, D.V., McGuire, R.E., von Rosenvinge, T.T., Kane, S.R., MacDowall, R.J.: 1989, Solar flare nuclear gamma rays and interplanetary proton events. *Astrophys. J.* **343**, 953. DOI. ADS.

Cliver, E.W., Kahler, S.W., Kazachenko, M., Shimojo, M.: 2019, The disappearing solar filament of 2013 September 29 and its large associated proton event: Implications for particle acceleration at the Sun. *Astrophys. J.* **877**, 11. DOI. ADS.

Cliver, E.W., Hayakawa, H., Love, J.J., Neidig, D.F.: 2020, On the size of the flare associated with the solar proton event in 774 AD. *Astrophys. J.* **903**, 41. DOI. ADS.

Croom, D.L.: 1971, Forecasting the intensity of solar proton events from the time characteristics of solar microwave bursts. *Solar Phys.* **19**, 171. DOI. ADS.

Dierckxsens, M., Tziotziou, K., Dalla, S., Patsou, I., Marsh, M.S., Crosby, N.B., Malandraki, O., Tsiropoula, G.: 2015, Relationship between solar energetic particles and properties of flares and CMEs: Statistical analysis of solar cycle 23 events. *Solar Phys.* **290**, 841. DOI. ADS.

Domingo, V., Fleck, B., Poland, A.I.: 1995, The SOHO mission: An overview. *Solar Phys.* **162**, 1. DOI. ADS.

Dulk, G.A., Marsh, K.A.: 1982, Simplified expressions for the gyrosynchrotron radiation from mildly relativistic, nonthermal and thermal electrons. *Astrophys. J.* **259**, 350. DOI. ADS.

Ellison, D.C., Ramaty, R.: 1985, Shock acceleration of electrons and ions in solar flares. *Astrophys. J.* **298**, 400. DOI. ADS.

Glesener, L., Krucker, S., Bain, H.M., Lin, R.P.: 2013, Observation of heating by flare-accelerated electrons in a solar coronal mass ejection. *Astrophys. J. Lett.* **779**, L29. DOI. ADS.

Gopalswamy, N., Xie, H., Yashiro, S., Akiyama, S., Mäkelä, P., Usoskin, I.G.: 2012, Properties of ground level enhancement events and the associated solar eruptions during solar cycle 23. *Space Sci. Rev.* **171**, 23. DOI. ADS.

Gopalswamy, N., Xie, H., Mäkelä, P., Yashiro, S., Akiyama, S., Uddin, W., Srivastava, A.K., Joshi, N.C., Chandra, R., Manoharan, P.K., *et al.*: 2013, Height of shock formation in the solar corona inferred from observations of type II radio bursts and coronal mass ejections. *Adv. Space Res.* **51**, 1981. DOI. ADS.

Gopalswamy, N., Mäkelä, P., Akiyama, S., Yashiro, S., Xie, H., Thakur, N., Kahler, S.W.: 2015, Large solar energetic particle events associated with filament eruptions outside of active regions. *Astrophys. J.* **806**, 8. DOI. ADS.

Grechnev, V.V., Kuzmenko, I.V.: 2020, A geoeffective CME caused by the eruption of a quiescent prominence on 29 September 2013. *Solar Phys.* **295**, 55. DOI. ADS.

Grechnev, V.V., Kurt, V.G., Chertok, I.M., Uralov, A.M., Nakajima, H., Altyntsev, A.T., Belov, A.V., Yushkov, B.Y., Kuznetsov, S.N., Kashapova, L.K., Meshalkina, N.S., Prestage, N.P.: 2008, An extreme solar event of 20 January 2005: Properties of the flare and the origin of energetic particles. *Solar Phys.* **252**, 149. DOI. ADS.

Grechnev, V.V., Uralov, A.M., Chertok, I.M., Kuzmenko, I.V., Afanasyev, A.N., Meshalkina, N.S., Kalashnikov, S.S., Kubo, Y.: 2011, Coronal shock waves, EUV waves, and their relation to CMEs. I. Reconciliation of "EIT waves", Type II radio bursts, and leading edges of CMEs. *Solar Phys.* **273**, 433. DOI. ADS.

Grechnev, V.V., Kiselev, V.I., Uralov, A.M., Meshalkina, N.S., Kochanov, A.A.: 2013a, An updated view of solar eruptive flares and the development of shocks and CMEs: History of the 2006 December 13 GLE-productive extreme event. *Publ. Astron. Soc. Japan* **65**, S9. DOI. ADS.

Grechnev, V.V., Meshalkina, N.S., Chertok, I.M., Kiselev, V.I.: 2013b, Relations between strong high-frequency microwave bursts and proton events. *Publ. Astron. Soc. Japan* **65**, S4. DOI. ADS.

Grechnev, V.V., Kiselev, V.I., Meshalkina, N.S., Chertok, I.M.: 2015, Relations between microwave bursts and near-Earth high-energy proton enhancements and their origin. *Solar Phys.* **290**, 2827. DOI. ADS.

Grechnev, V.V., Kiselev, V.I., Uralov, A.M., Klein, K.-L., Kochanov, A.A.: 2017a, The 26 December 2001 solar eruptive event responsible for GLE63: III. CME, shock waves, and energetic particles. *Solar Phys.* **292**, 102. DOI. ADS.

Grechnev, V.V., Lesovoi, S.V., Kochanov, A.A., Uralov, A.M., Altyntsev, A.T., Gubin, A.V., Zhdanov, D.A., Ivanov, E.F., Smolkov, G.Y., Kashapova, L.K.: 2018, Multi-instrument view on solar eruptive events observed with the Siberian Radioheliograph: From detection of small jets up to development of a shock wave and CME. *J. Atm. Solar-Terr. Phys.* **174**, 46. DOI. ADS.

Grechnev, V.V., Kochanov, A.A., Uralov, A.M., Slemzin, V.A., Rodkin, D.G., Goryaev, F.F., Kiselev, V.I., Myshyakov, I.I.: 2019, Development of a fast CME and properties of a related interplanetary transient. *Solar Phys.* **294**, 139. DOI. ADS.

Grechnev, V., Uralov, A.M., Kiselev, V.I., Kochanov, A.A.: 2017b, The 26 December 2001 solar eruptive event responsible for GLE63. II. Multi-loop structure of microwave sources in a major long-duration flare. *Solar Phys.* **292**, 3. DOI. ADS.

Hannah, I.G., Kontar, E.P.: 2011, The spectral difference between solar flare HXR coronal and footpoint sources due to wave-particle interactions. *Astron. Astrophys.* **529**, A109. DOI. ADS.

Harper, W.V.: 2016, *Reduced Major Axis Regression*, John Wiley & Sons, Ltd, 1. DOI. https://onlinelibrary.wiley.com/doi/abs/10.1002/9781118445112.stat07912.

Kahler, S.W.: 1982, The role of the big flare syndrome in correlations of solar energetic proton fluxes and associated microwave burst parameters. *J. Geophys. Res.* **87**, 3439. DOI. ADS.

Kahler, S.W., Kazachenko, M., Lynch, B.J., Welsch, B.T.: 2017, Flare magnetic reconnection fluxes as possible signatures of flare contributions to gradual SEP events. In: *J. Phys. Conf. Ser.* **900**, 012011. DOI. ADS.

Kallenrode, M.-B.: 2003, Current views on impulsive and gradual solar energetic particle events. *J. Phys. G Nuclear Phys.* **29**, 965. ADS.

Kane, S.R.: 1974, Impulsive (flash) phase of solar flares: Hard X-ray, microwave, EUV and optical observations. In: Newkirk, G.A. (ed.) *Coronal Disturbances* **57**, 105. ADS.

Klein, K.-L.: 2021, Radio astronomical tools for the study of solar energetic particles II.Time-extended acceleration at subrelativistic and relativistic energies. *Frontiers in Astronomy and Space Sciences* **7**, 93. DOI. ADS.

Klein, K.-L., Trottet, G.: 2001, The origin of solar energetic particle events: coronal acceleration versus shock wave acceleration. *Space Sci. Rev.* **95**, 215. ADS.

Kocharov, L., Pohjolainen, S., Mishev, A., Reiner, M.J., Lee, J., Laitinen, T., Didkovsky, L.V., Pizzo, V.J., Kim, R., Klassen, A., Karlicky, M., Cho, K.-S., Gary, D.E., Usoskin, I., Valtonen, E., Vainio, R.: 2017, Investigating the origins of two extreme solar particle events: Proton source profile and associated electromagnetic emissions. *Astrophys. J.* **839**, 79. DOI. ADS.

Koldobskiy, S., Raukunen, O., Vainio, R., Kovaltsov, G.A., Usoskin, I.: 2021, New reconstruction of event-integrated spectra (spectral fluences) for major solar energetic particle events. *Astron. Astrophys.* **647**, A132. DOI. ADS.

Kundu, M.R., Grechnev, V.V., White, S.M., Schmahl, E.J., Meshalkina, N.S., Kashapova, L.K.: 2009, High-energy emission from a solar flare in hard X-rays and microwaves. *Solar Phys.* **260**, 135. DOI. ADS.

Kuznetsov, S.N., Kurt, V.G., Myagkova, I.N., Yushkov, B.Y., Kudela, K.: 2006, Gamma-ray emission and neutrons from solar flares recorded by the SONG instrument in 2001–2004. *Solar Sys. Res.* **40**, 104. DOI. ADS.

Kuznetsov, S.N., Kurt, V.G., Yushkov, B.Y., Kudela, K., Galkin, V.I.: 2011, Gamma-ray and high-energy-neutron measurements on CORONAS-F during the solar flare of 28 October 2003. *Solar Phys.* **268**, 175. DOI. ADS.

Kuznetsov, S.N., Kurt, V.G., Yushkov, B.Y., Myagkova, I.N., Galkin, V.I., Kudela, K.: 2014, In: Kuznetsov, V. (ed.) *Protons acceleration in solar flares: The results of the analysis of gamma-emission and neutrons recorded by the SONG instrument onboard the CORONAS-F satellite* **400**, 301. DOI. ADS.

Li, G., Lee, M.A.: 2015, Scatter-dominated interplanetary transport of solar energetic particles in large gradual events and the formation of double power-law differential fluence spectra of ground-level events during Solar Cycle 23. *Astrophys. J.* **810**, 82. DOI. ADS.

Lin, R.P., Dennis, B.R., Hurford, G.J., Smith, D.M., Zehnder, A., Harvey, P.R., Curtis, D.W., Pankow, D., Turin, P., Bester, M., *et al.*: 2002, The Reuven Ramaty High-Energy Solar Spectroscopic Imager (RHESSI). *Solar Phys.* **210**, 3. DOI. ADS.

Logachev, Y.I., Bazilevskaya, G.A., Vashenyuk, E.V., Daibog, E.I., Ishkov, V.N., Lazutin, L.L., Miroshnichenko, L.I., Nazarova, M.N., Petrenko, I.E., Stupishin, A.G., Surova, G.M., Yakovchuk, O.S.: 2016, *Catalogue of solar proton events in the 23rd cycle of solar activity*, Geophysical Center RAS, Moscow, Russia (www.gcras.ru/eng/), Moscow. DOI.

Masson, S., Antiochos, S.K., DeVore, C.R.: 2013, A model for the escape of solar-flare-accelerated particles. *Astrophys. J.* **771**, 82. DOI. ADS.

McCracken, K.G., Moraal, H., Stoker, P.H.: 2008, Investigation of the multiple-component structure of the 20 January 2005 cosmic ray ground level enhancement. *J. Geophys. Res. (Space Physics)* **113**, A12101. DOI. ADS.

Melnikov, V.F., Podstrigach, T.S., Dajbog, E.I., Stolpovskij, V.G.: 1991, Nature of the relationship between the fluxes of solar cosmic ray electrons and protons and the parameters of microwave bursts. *Cosmic Res.* **29**, 87. ADS.

Metcalf, T.R., Alexander, D.: 1999, Coronal trapping of energetic flare particles: Yohkoh/HXT observations. *Astrophys. J.* **522**, 1108. DOI. ADS.

Mewaldt, R.A., Looper, M.D., Cohen, C.M.S., Haggerty, D.K., Labrador, A.W., Leske, R.A., Mason, G.M., Mazur, J.E., von Rosenvinge, T.T.: 2012, Energy spectra, composition, and other properties of ground-level events during solar cycle 23. *Space Sci. Rev.* **171**, 97. DOI. ADS.

Miller, J.A., Ramaty, R.: 1989, Relativistic electron transport and bremsstrahlung production in solar flares. *Astrophys. J.* **344**, 973. DOI. ADS.

Miroshnichenko, L.: 2015, *Solar Cosmic Rays* **405**. DOI. ADS.

Moraal, H., McCracken, K.G.: 2012, The time structure of ground level enhancements in Solar Cycle 23. *Space Sci. Rev.* **171**, 85. DOI. ADS.

Núñez, M., Klein, K.-L., Heber, B., Malandraki, O.E., Zucca, P., Labrens, J., Reyes-Santiago, P., Kuehl, P., Pavlos, E.: 2018, HESPERIA forecasting tools: Real-time and post-event. In: Malandraki, O.E., Crosby, N.B. (eds.) *Solar Particle Radiation Storms Forecasting and Analysis*, *Astrophysics and Space Science Library* **444**, 113. DOI. ADS.

Ogawara, Y., Takano, T., Kato, T., Kosugi, T., Tsuneta, S., Watanabe, T., Kondo, I., Uchida, Y.: 1991, The SOLAR-A mission - An overview. *Solar Phys.* **136**, 1. DOI. ADS.

Papaioannou, A., Sandberg, I., Anastasiadis, A., Kouloumvakos, A., Georgoulis, M.K., Tziotziou, K., Tsiropoula, G., Jiggens, P., Hilgers, A.: 2016, Solar flares, coronal mass ejections and solar energetic particle event characteristics. *J. Space Weather Space Climate* **6**, A42. DOI. ADS.

Reames, D.V.: 2009, Solar release times of energetic particles in ground-level events. *Astrophys. J.* **693**, 812. DOI. ADS.

Reames, D.V.: 2013, The two sources of solar energetic particles. *Space Sci. Rev.* **175**, 53. DOI. ADS.

Sato, J., Matsumoto, Y., Yoshimura, K., Kubo, S., Kotoku, J., Masuda, S., Sawa, M., Suga, K., Yoshimori, M., Kosugi, T., Watanabe, T.: 2006, YOHKOH/WBS recalibration and a comprehensive catalogue of solar flares observed by YOHKOH SXT, HXT and WBS instruments. *Solar Phys.* **236**, 351. DOI. ADS.

Share, G.H., Murphy, R.J., White, S.M., Tolbert, A.K., Dennis, B.R., Schwartz, R.A., Smart, D.F., Shea, M.A.: 2018, Characteristics of late-phase $>$ 100 MeV gamma-ray emission in solar eruptive events. *Astrophys. J.* **869**, 182. DOI. ADS.

Sladkova, A.I., Bazilevskaya, G.A., Ishkov, V.N., Nazarova, M.N., Pereyaslova, N.K., Stupishin, A.G., Ulyev, V.A., Chertok, I.M.: 1998, *Catalogue of solar proton events 1987–1996*, Geophysical Center RAS, Moscow, Russia (www.gcras.ru/eng/), Moscow. DOI.

Smith, D.M., Lin, R.P., Turin, P., Curtis, D.W., Primbsch, J.H., Campbell, R.D., Abiad, R., Schroeder, P., Cork, C.P., Hull, E.L., Landis, *et al.*: 2002, The RHESSI spectrometer. *Solar Phys.* **210**, 33. DOI. ADS.

Tan, L.C., Malandraki, O.E., Reames, D.V., Ng, C.K., Wang, L., Patsou, I., Papaioannou, A.: 2013, Comparison between path lengths traveled by solar electrons and ions in ground-level enhancement events. *Astrophys. J.* **768**, 68. DOI. ADS.

Tolbert, K., Schwartz, R.: 2020, *OSPEX: Object Spectral Executive*. ADS.

Tripathi, S.C., Khan, P.A., Aslam, A.M., Gwal, A.K., Purohit, P.K., Jain, R.: 2013, Investigation on spectral behavior of solar transients and their interrelationship. *Astrophys. Spa. Sci.* **347**, 227. DOI. ADS.

Trottet, G., Samwel, S., Klein, K.-L., Dudok de Wit, T., Miteva, R.: 2015, Statistical evidence for contributions of flares and coronal mass ejections to major solar energetic particle events. *Solar Phys.* **290**, 819. DOI. ADS.

Tylka, A.J., Dietrich, W.F.: 2009, A new and comprehensive analysis of proton spectra in ground-level enhanced (GLE) solar particle events. In: *31st Internat. Cosmic Ray Conf. (ICRC 2009)* **4**, 2953.

Tylka, A.J., Cohen, C.M.S., Dietrich, W.F., Lee, M.A., Maclennan, C.G., Mewaldt, R.A., Ng, C.K., Reames, D.V.: 2005, Shock geometry, seed populations, and the origin of variable elemental composition at high energies in large gradual solar particle events. *Astrophys. J.* **625**, 474. DOI. ADS.

Uralov, A.M., Grechnev, V.V., Ivanukin, L.A.: 2019, Self-similar piston-shock and CME. *Solar Phys.* **294**, 113. DOI. ADS.

Vashenyuk, E.V., Balabin, Y.V., Miroshnichenko, L.I., Perez-Peraza, J., Gallegos-Cruz, A.: 2008, Relativistic solar cosmic ray events (1956-2006) from GLE modeling studies. In: *Internat. Cosmic Ray Conf.* **1**, 253. ADS.

Vilmer, N., MacKinnon, A.L., Hurford, G.J.: 2011, Properties of energetic ions in the solar atmosphere from γ-ray and neutron observations. *Space Sci. Rev.* **159**, 167. DOI. ADS.

Yashiro, S., Gopalswamy, N., Michalek, G., St. Cyr, O.C., Plunkett, S.P., Rich, N.B., Howard, R.A.: 2004, A catalog of white light coronal mass ejections observed by the SOHO spacecraft. *J. Geophys. Res. (Space Physics)* **109**, A07105. DOI. ADS.

Yoshimori, M., Okudaira, K., Hirasima, Y., Igarashi, T., Akasaka, M., Takai, Y., Morimoto, K., Watanabe, T., Ohki, K., Nishimura, J., Yamagami, T., Ogawara, Y., Kondo, I.: 1991, The Wide Band Spectrometer on the SOLAR-A. *Solar Phys.* **136**, 69. DOI. ADS.

Yu, X.X., Lu, H., Chen, G.T., Li, X.Q., Shi, J.K., Tan, C.M.: 2015, Detection of solar neutron events and their theoretical approach. *New Astron.* **39**, 25. DOI. ADS.

Zhao, L., Zhang, M., Rassoul, H.K.: 2016, Double power laws in the event-integrated solar energetic particle spectrum. *Astrophys. J.* **821**, 62. DOI. ADS.